Fracture and self-sensing characteristics of super-fine stainless wire reinforced reactive powder concrete

Sufen Dong[1], Xufeng Dong[1], Ashraf Ashour[2], Baoguo Han[3, *], Jinping Ou[3]

[1] *School of Material Science and Engineering, Dalian University of Technology, Dalian, 116024 China*
[2] *Faculty of Engineering & Informatics, University of Bradford, Bradford, BD7 1DP, UK*
[3] *School of Civil Engineering, Dalian University of Technology, Dalian, 116024 China*
* Corresponding author: hithanbaoguo@163.com, hanbaoguo@dlut.edu.cn

Abstract:

Super-fine stainless wire (SSW) can not only form widely distributed enhancing, toughening and conductive network in reactive powder concrete (RPC) at low dosage level, but also improve weak interface area and refine cracks due to its micron scale diameter and large specific surface. In addition, the crack resistance zone generated by SSWs and RPC matrix together has potential to further enhance the fracture properties of composites. Therefore, fracture and self-sensing characteristics of SSW reinforced RPC composites were investigated in this paper. Experimental results indicated that adding 1.5 vol. % of SSW leads to 183.1% increase in the initial cracking load of RPC specimens under three-point bending load. Based on two parameter fracture model calculations, an increase of 203.4% in fracture toughness as well as an increase of 113.3% in crack tip opening displacement of the composites reinforced with 1.5% SSWs are achieved. According to double-*K* fracture model calculations, the initiation fracture toughness and unstable fracture toughness of the composites are enhanced by 185.2% and 179.2%, respectively. The increment for fracture energy of the composites reaches up to 1017.1% because of the emergence of blunt and tortuous cracks. The mixed mode I-II fracture toughness of the composites is increased by 177.1% under four-point shearing load. The initial angle of mixed mode I-II cracks of the composites decreases with the increase of SSW content. The initiation and propagation of cracks in the composites can be monitored by their change in electrical resistivity. The excellent fracture toughness of the composites is of great significance for the improvement of

structure safety in serviceability limit states, and the self-sensing ability of the composites can also provide early warning for the degradation of structure safety.

Key words: Super-fine stainless wire; reactive powder concrete; fracture toughness; fracture energy; fracture self-sensing

1 Introduction

Due to the brittleness characteristic and low deformation capacity of concrete, cracks and defects in concrete are inevitable, reducing the durability of concrete structures, leading eventually to the collapse of structures. Hence, the causes of cracks in concrete structures, crack initiation, propagation, and prevention are of great concern in engineering fields. Ultra-high performance concrete, e.g., reactive powder concrete (RPC), has been widely used in long-span, ultrahigh-rise and complex civil engineering infrastructures in order to improve the safety and applicability of structures. Despite of their excellent mechanical properties, the propagation of cracks still plays a crucial role in the safety of RPC structures.

The emergence of fracture mechanics provides an important tool for the investigation of concrete crack propagation. The concept of fracture mechanics of brittle material was firstly put forward by Griffith [1]. In 1961, Kaplan applied linear elastic fracture mechanics (LEFM) to investigate crack propagation and fracture of concrete [2]. Since then, a large number of fracture tests have been conducted on concrete, proposing many modified LEFM models, such as two parameter fracture model (TPFM) [3], equivalent crack fracture model (ECFM) [4] and double-K fracture model (DKFM) [5]. In these above models, the fracture toughness and fracture energy are established to evaluate mode I fracture characteristics of concrete using a notched three-point bending beam test as mode I cracks - opening mode cracks - are the most

dangerous and most likely to cause low-stress brittle failure within structural elements. Cracks in concrete structure are also typically under bending-shear combined stress fields because of asymmetries of structural geometries and complexities of loading conditions, resulting in the occurrence of mixed mode I-II (opening-sliding) cracks [6].

The fracture characteristics and mechanisms of concrete structures with mode I and mixed mode I-II cracks have important engineering significance and attracted vast amount of research investigations. Ghasemi et al. [7] concluded that fracture energy of self-compacting concrete increases by up to 112.4% due to the addition of steel fibers of 0.6 mm diameter and 30 mm length, whereas the energy absorption and ductility of self-compacting concrete enhance with the increasing fiber content (0.1-0.5 vol.%). Kazemi et al. [8] showed that fracture energy of high strength concrete can reach 6871 J/m^2 when the volume fraction of hooked-end steel fiber is added by up to 1.6%, but Noaman et al. [9] found that fracture energy of concrete is improved by 152% with the addition of 0.5% by volume of hooked-end steel fiber. Meanwhile, in the research of Kazemi et al. [8], most of steel fibers in high strength concrete are ruptured once failure occurred because of the high bond strength between matrix and fibers. Sovjáka et al. [10] concluded that fracture energy of super-high performance fiber-reinforced concrete increases as the aspect ratio of steel fiber increases, reaching 32400 J/m^2 when the aspect ratio of steel fibers (0.13 mm diameter and 14 mm length) is 108:1. Güneyisi et al. [11] determined the fracture energy of steel fiber reinforced artificial lightweight aggregate concrete according to the recommendation of RILEM 50-FMC Technical Committee. The steel fiber with aspect ratio of 80 exhibits the most efficient result for fracture energy. The fracture energy value can be increased by 280 times and reach 10754.5 J/m^2. Mo et al. [12] found that the fracture energy is enhanced by almost 3 times when steel fibers are added from 0.5% to 1.0% volume fraction, and the fracture

toughness increases from 0.563 MPa·m$^{1/2}$ to 1.877 MPa·m$^{1/2}$. The improvement of fracture performance can be attributed to the mechanism of steel fiber diverting crack path, preventing direct propagation of cracks and undergoing de-bonding with concrete matrix. Su et al. [13] performed semi-circular bend test on RPC to investigate the mode I fracture characteristics. The results showed that the fracture energy has risen from 102 J/m^2 to 8984 J/m^2 and the fracture toughness has increased to 3.71 MPa·m$^{1/2}$ from 0.88 MPa·m$^{1/2}$ due to the inclusion of 4% volume fraction of steel fiber (with diameter of 0.22 mm). The fracture toughness and fracture energy of RPC are proportional to steel fiber content. Xu and Wille [14] found that the fracture energy of ultra-high performance fiber reinforced concrete with 1.5-3 vol.% steel fiber can reach up to 12-29 kJ/m^2 due to the high strength of concrete matrix, and the interfacial bond strength of straight, end hooked and twisted steel fibers with the enhanced concrete matrix is similar. Köksal et al. [15] concluded that concrete matrix and steel fiber tensile strength need to adapt to each other in order to obtain concrete with high fracture energy. Steel fibers with a low tensile strength exhibit high fracture energy for low concrete matrix while steel fibers with a high tensile strength is conductive to the improvement of fracture energy for high concrete matrix. Bencardino et al. [16] evaluated the fracture behavior of steel fiber reinforced concrete using three-point bending test and four-point bending test, respectively. Steel fiber reinforced concrete specimens under four-point bending load show higher stress values than that under three-point bending load. The post-peak behavior of high strength concrete is improved by the incorporation of steel fibers. Dai et al. [17] verified the feasibility of electronic speckle pattern interferometry in measuring the fracture process zone of steel fiber reinforced concrete beams. Mudadu et al. [18] found that the fracture energy obtained by horizontally cast steel fiber reinforced concrete beams under three-point bending load is higher than that of

vertically cast samples under uniaxial tensile load, and verified that the post-cracking performance of steel fiber reinforced concrete is significantly affected by fiber orientation. In addition, the experimental methods and theoretical analysis on the mixed mode I-II fracture behaviors of concrete have been widely studied by many researches [19-21].

It can be known from the above summary that steel fiber especially hooked-end steel fiber has remarkable reinforcing effect on the fracture performances of concrete [9-21]. Meanwhile, the fracture toughening effect of micro steel fiber on RPC can be achieved at high volume fraction [13]. Nevertheless, adding normal steel fibers (with diameter larger than 0.2 mm) into concrete has certain disadvantages such as reduced workability, extended mixing and placing time, unobvious mechanical enhancement effect at low dosage and weak interfacial transition zone between steel fiber and concrete matrix [22-24], which greatly limits the applications of concrete. Owing to its micron diameter and high aspect ratio, super-fine stainless wire (SSW) can not only form three-dimensional disordered network in RPC at low dosage level, but also enhance the microstructure of RPC and weaken the adverse effect of interface transition zone. This enables that the SSW reinforced RPC presents good workability, mechanical behavior and multi-functional property [25-28]. In addition, the existence of crack resistance zone formed by SSWs and RPC matrix together is crucial for inhibiting the initiation and propagation of cracks, leading to significant enhancement of fracture characteristics of the composites. Meanwhile, multi-functional/smart concrete not only has the potential in detecting strain, stress, crack and damage under static and dynamic load, but also can be used for traffic detecting, rebar corrosion monitoring and structural vibration control, leading to the sustainable development of concrete infrastructures [29-33]. The conductive pathway composed of overlapped SSWs will endow RPC with

the ability to sense the development of cracks. Therefore, the notched beam specimens of SSW reinforced RPC were tested under three-point bending and four-point shearing load in order to investigate mode I and mixed mode I-II fracture behaviors of the composites in this paper. In addition, the self-sensing characteristics of the composites were investigated and the inhibiting and bridging effect of SSWs on the initiation and propagation of cracks was analyzed.

2 Experimental schemes

2.1 Raw materials and mix proportion

The properties of raw materials including super-fine stainless wire (SSW), cement, silica fume, fly ash, and quartz sand used in this paper were the same as that in references [25] and [26]. The diameter of SSW was 20 μm and the length was 10 mm. The mix proportion of control RPC was determined on the basis of that proposed by Richard [34] in 1995. The mix proportion of (cement: silica fume: quartz sand: water) equaled to (1:0.25:1.1:0.3), of which the percentage replacement of cement with fly ash was 20%. Three volume fractions of SSW, namely 0%, 1% and 1.5%, were investigated, labelled as W0, W201010 and W201015, respectively. W0 is the RPC without SSW, W201010 and W201015 are representative of RPC composites reinforced with 1% and 1.5% SSWs, respectively. In order to ensure the fluidity of the composites (the fluidity value obtained by cement mortar fluidity tester was 210±10 mm), the dosage of superplasticizer was adjusted according to the volume fraction of SSW.

2.2 Specimens preparation

Three-point bending and four-point shearing notched beam methods were employed to identify mode I and mixed mode I-II fracture parameters of SSW reinforced RPC. The size of beam specimens with initial precast crack (width

approximately 3 mm, and depth of 10 mm and 20 mm) was 40 mm×40 mm×160 mm. The corresponding crack length/depth ratio (a_0/h) was 0.25 and 0.5, respectively.

The mixing process of the composites was conducted according to references [25] and [26]. A 10 mm or 20 mm height flat steel plate having a 3 mm thickness was prepositioned at the middle of the molds to achieve the middle notch during casting of specimens. Two stainless steel gauze electrodes (with size of 40 mm×40 mm×60 mm) were embedded in the corresponding position of specimens (10 mm measured from one side of specimens) to achieve the required connections for detecting the self-sensing properties of RPC composites. The mixtures of SSW reinforced RPC were put into oiled molds in one-go, that were vibrated for two minutes on the concrete vibration table. Next, all specimens were kept in a standard curing chamber and then demoulded after 24 hours. The specimens were put into accelerating curing box for 48 hours (the water temperature was 90 °C and temperature increase/decrease rate was 15°C/h), then, the specimens were placed in room temperature environment for 28 days for curing before testing.

2.3 Measurement of fracture behaviors

The schematic programs of three-point bending and four-point shearing fracture tests were plotted in Fig.1. The tests were conducted under displacement control arrangement and the loading rate was 0.05 mm/min. As demonstrated in Fig.1 (a), a linearly varying displacement transducer (LVDT) was used to measure the mid-span deflection as the three-point bending load was applied by an electronic universal testing machine. The fracture energy was calculated on the basis of load-deflection curves. Fig.1 also shows that a clip gauge attached to knife edges glued to the specimens was connected to a data acquisition system (DH 3820) in order to measure the crack mouth opening displacement (CMOD) of composites under three-point bending and four-point

shearing load. The strain gauges (BX120-20AA, produced by Zhejiang Huangyan Testing Apparatus Factory) were pasted on both sides and the upper end of the initial notch of specimens in order to get the initial cracking load and critical effective crack length of composites, as shown in Fig.2. Dynamic strain indicator DC-204R provided by Tokyo Sokki Kenkyujo Co., Ltd. was employed to acquire strains at different locations. Meanwhile, the two-electrode-DC resistance measurement during the load process was carried out by using Keithley 2100. The electrical resistivity, ρ, is calculated according to $\rho=RS/L$ (where ρ is electrical resistivity, R is electrical resistance, S is cross sectional area, and L is the distance between two electrodes). The fractional change in electrical resistivity (FCR) is calculated based on $\Delta\rho = 100\% \times (\rho_l - \rho_0)/\rho_0$, where ρ_0 is the resistivity without loading, ρ_l is the resistivity under loading.

There were three identical specimens for each concrete mix. The load-deflection curve closest to the average one was selected to analyze the deformation capacity of SSW reinforced RPC. The curves of load-CMOD, load-strain and load-FCR were selected by the same method. The initial cracking load, measured critical effective crack length, three-point bending fracture toughness and fracture energy were calculated based on the above selected curves in order to ensure the consistency of result analysis. The average value of four-point shear force and four-point shearing fracture toughness of three specimens for each concrete mix was regarded as the final result if the difference between average and the maximum and the minimum value was less than 15%. The sampling rate of stress, strain, deflection, CMOD and FCR was 2 Hz.
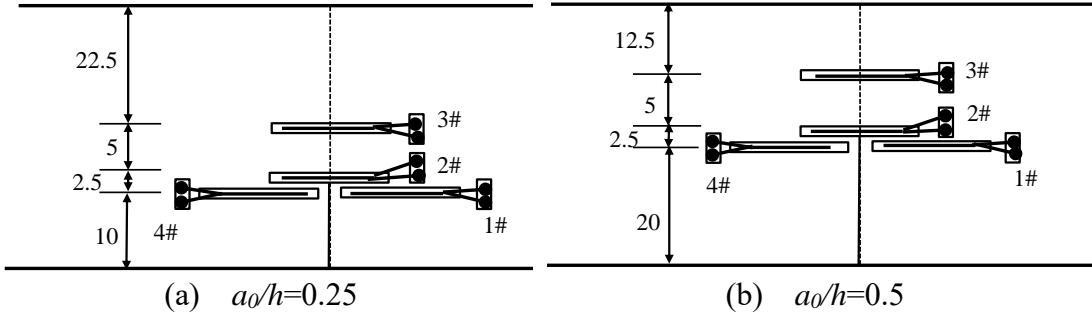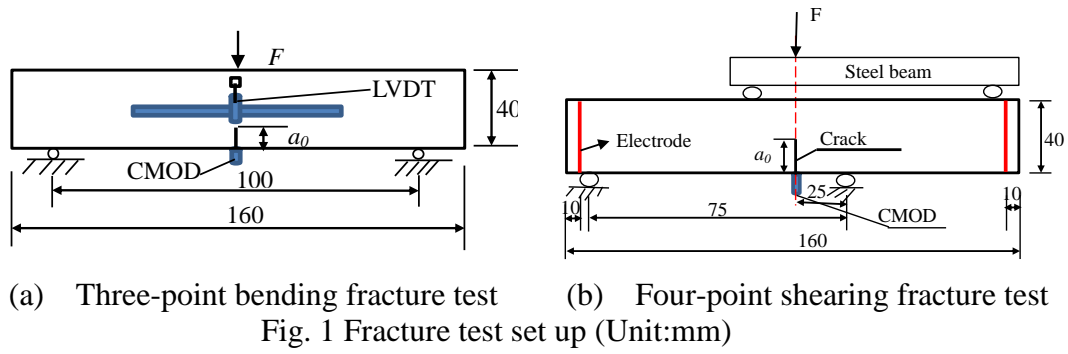
(a) Three-point bending fracture test   (b) Four-point shearing fracture test

Fig. 1 Fracture test set up (Unit:mm)

(a) a_0/h=0.25   (b) a_0/h=0.5

Fig. 2   Strain gauges layout for different crack length/depth ratios (Unit:mm)

3 Three-point bending fracture behaviors

3.1 Load-deflection and Load-CMOD curves

Fig.3 shows the load-deflection curves of SSW reinforced RPC at different crack length/depth ratios. As can be seen from Fig.3, the peak and limit values of deflections of RPC are enhanced because of the incorporation of SSW. The linear elastic stage of load-deflection curves for composites is prolonged, which can be attributed to the dense structure and refined grain of RPC matrix caused by SSW. The load-deflection curves show nonlinearity when the deformation of RPC matrix reaches the initial cracking strain. The non-linear ascending stage of the curves becomes more obvious with the increase of SSW volume fraction. During this stage, the generation of new cracks and the propagation of original cracks are hindered by RPC matrix and SSWs together. When the cracks become saturate to form localized failure cracks, the load reaches the peak and, then, decreases slowly. The bridging effect of SSW endows a slow descending stage for the load-deflection curves of RPC. The failure cracks continue to

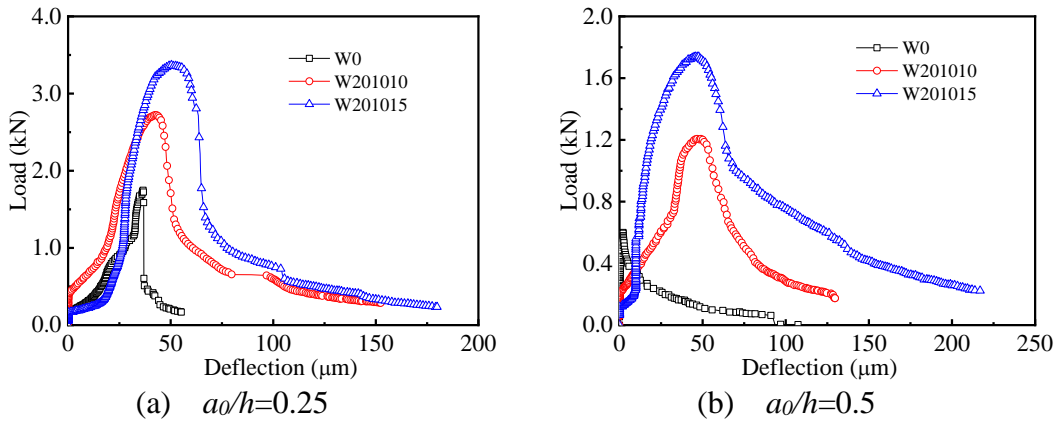open and the SSWs are ruptured gradually with the load decrease.

(a) a_0/h=0.25   (b) a_0/h=0.5

Fig. 3 Load-deflection curves of SSW reinforced RPC under three-point bending load

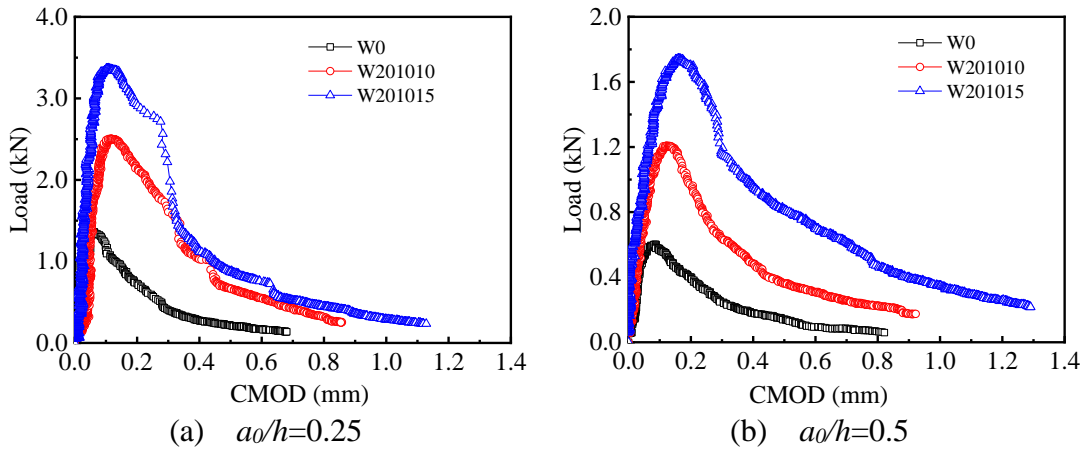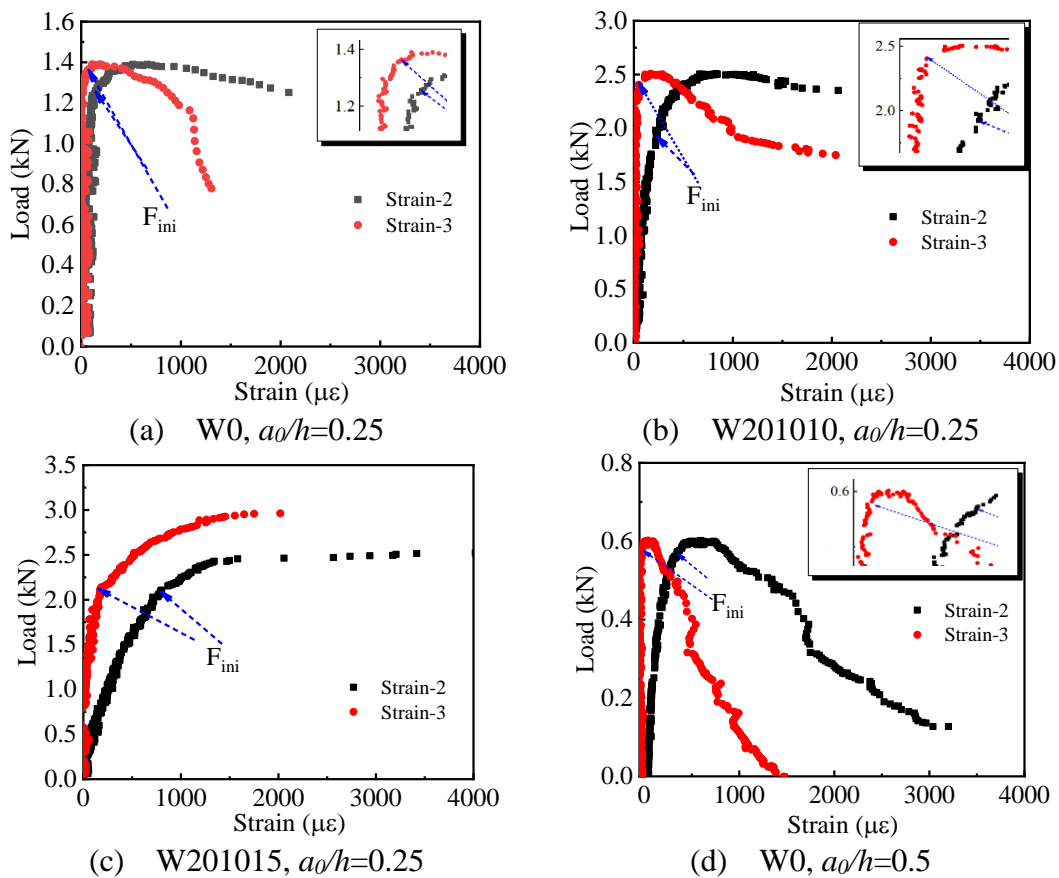(a) a_0/h=0.25   (b) a_0/h=0.5

Fig. 4 Load-CMOD curves of SSW reinforced RPC under three-point bending load

The load-CMOD curves of SSW reinforced RPC are demonstrated in Fig.4. At the crack length/depth ratio of 0.25, the peak load and peak CMOD ($COMD_C$) of RPC are improved by 84.6%, 147.8% and 86.3%, 74.5% respectively due to the addition of 1% and 1.5% SSWs. The corresponding enhancement ratios are 108.3%, 190.0% and 42.3%, 85.9% respectively at the crack length/depth ratio of 0.5. The main features of load-CMOD curves for the composites are independent of crack length/depth ratio. The prolongation of linear ascending stage of load-CMOD curves indicates the enhanced resistance of RPC matrix to cracking. With the increase of SSW volume fraction, the slope of non-linear ascending stage drops obviously, the descending stage becomes

gently, and the limit value of CMOD is improved remarkably. This phenomenon can be attributed to the bridging effect of SSW in RPC.

3.2 Measured critical effective crack length

The critical effective crack length (a_c) is defined as the crack length of concrete specimens in failure state, which can be monitored by strain gauges arranged on the upper end of the precast crack. The variation of strains obtained by strain gauge-2 and strain gauge-3 are shown in Fig.5. Fig.5 demonstrates that SSW reinforced RPC where the strain gauge is located has been cracking as the load-strain curves step into non-linear ascending stage. The limit values of strain are enhanced with the increase of SSW volume fraction, and the composite specimens still have certain bearing capacity after cracking due to the bridging effect of SSWs.

(a) W0, a_0/h=0.25

(b) W201010, a_0/h=0.25

(c) W201015, a_0/h=0.25

(d) W0, a_0/h=0.5

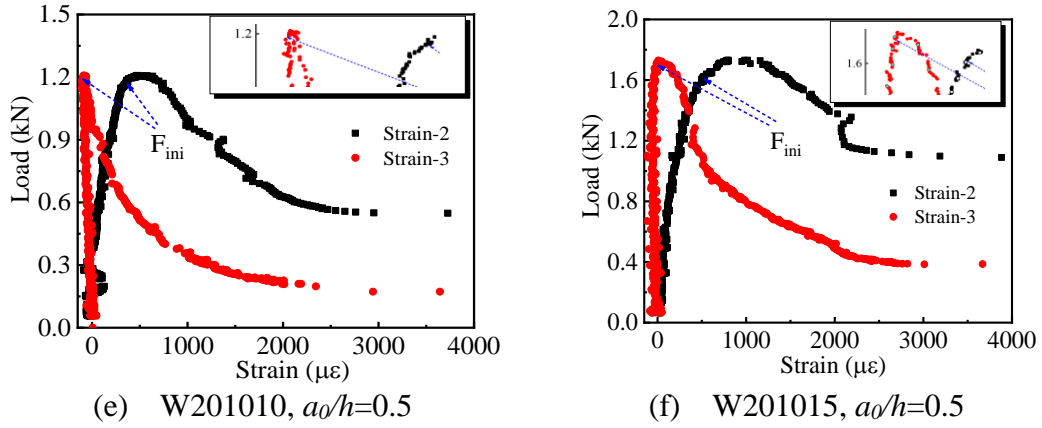(e)　W201010, a_0/h=0.5　　　　(f)　W201015, a_0/h=0.5

Fig. 5 Monitoring strain of SSW reinforced RPC under three-point bending load

The cracking load, cracking time and critical effective crack length of SSW reinforced RPC are displayed in Table 1. The cracking loads for the locations of strain gauge-2 and strain gauge-3 increase with SSW volume fraction increasing. At the crack length/depth ratio of 0.25, the cracking load for strain gauge-2 location of RPC without SSW is 0.57 kN which increases to 1.79 kN and 2.04 kN for RPC reinforced with 1% and 1.5% SSWs, indicating 214.0% and 257.9% enhancement, respectively. Meanwhile, the cracking load for strain gauge-3 location of composites exhibits 110.5% and 87.7% improvements. At the crack length/depth ratio of 0.5, the cracking load for strain gauge-2 location of SSW reinforced RPC exceeds that of control RPC by 101.8% and 171.9%, and the load value for strain gauge-3 location of composites exhibits 105.8% and 176.3% greater than the control. The enhancement of cracking load represents the inhibiting and bridging effect of SSW to macro cracks.

The cracking interval time between the locations of strain gauge-2 and strain gauge-3 for RPC without SSW is 83 s at crack length/depth ratio of 0.25, and that between the locations of strain gauge-3 and peak load is 28.5 s while the load difference is 0.22 kN. The unstable crack has surpassed the location of strain gauge-3. Therefore, the measured critical crack length of control RPC is larger than 27.5 mm. The cracking

interval time between the locations of strain gauge-2 and strain gauge-3 for RPC reinforced with 1% SSWs is 53.5 s, and that between the locations of strain gauge-3 and peak load is 14.5 s while the load difference is only 0.11 kN. The multiple cracking characteristic of SSW reinforced RPC shortens the time of crack stable and unstable propagation. The measured critical crack length is also larger than 27.5 mm. The above two cracking interval times for RPC reinforced with 1.5% SSWs are 6 s and 86 s, respectively. The cracking interval time between the locations of strain gauge-2 and strain gauge-3 is shorten due to the occurrence of multiple micro cracks, and the prolongation of cracking interval time between the locations of strain gauge-3 and peak load can be attributed to the bridging effect of SSWs on crack propagation. The measured critical crack length is about 27.5 mm.

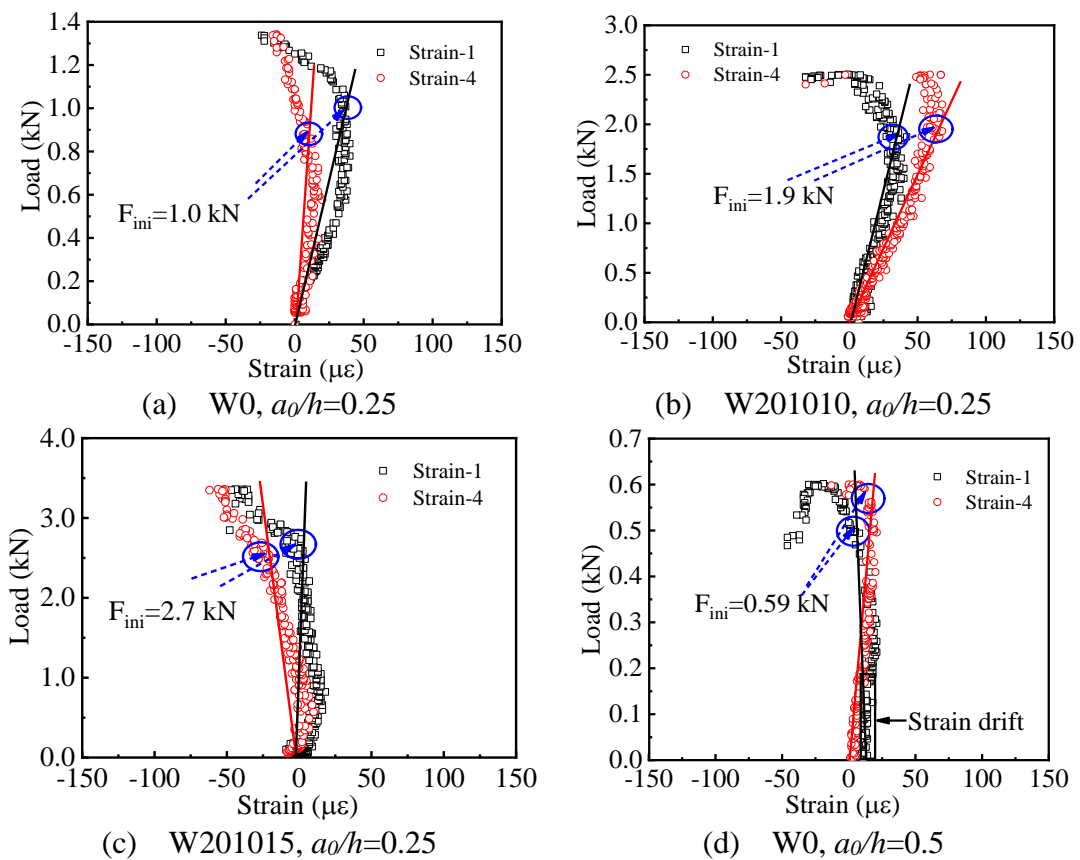Table 1 Measured critical crack length of SSW reinforced RPC

Specimens			Position /mm	Cracking time /s	Cracking load/kN	Peak load/kN	Peak load time/s	a_c/mm
a_0/h=0.25	W0	Strain-2	12.5	349.5	0.57	1.36	461.0	>27.5
		Strain-3	27.5	432.5	1.14			
	W201010	Strain-2	12.5	327.5	1.79	2.51	395.5	>27.5
		Strain-3	27.5	381.0	2.40			
	W201015	Strain-2	12.5	460.5	2.04	3.37	552.5	≈27.5
		Strain-3	27.5	466.5	2.14			
a_0/h=0.5	W0	Strain-2	22.5	347.5	0.57	0.60	352.5	<32.5
		Strain-3	37.5	351.5	0.59			
	W201010	Strain-2	22.5	363.5	1.15	1.25	379.0	≈32.5
		Strain-3	37.5	377.5	1.21			
	W201015	Strain-2	22.5	334.0	1.55	1.74	370.5	≈32.5
		Strain-3	37.5	343.0	1.63			

At the crack length/depth ratio of 0.5, the load-strain curves of SSW reinforced RPC possess complete descending stage. Therefore, the measurement of critical effective crack length is bounded by geometric center line of strain gauge-3. The cracking interval time between the locations of strain gauge-2 and strain gauge-3 for composites is 4 s, 14 s and 9 s, and that between the locations of strain gauge-3 and peak load is 1 s, 1.5 s and 27.5 s, respectively. The peak load of control RPC is only 0.6 kN and the critical effective crack length is smaller than 32.5 mm. The cracking loads for the locations of strain gauge-3 and peak load of RPC reinforced with 1% SSWs are only separated by 0.04 kN. The cracks have entered into the unstable propagation stage at the location of stain gauge-3. Therefore, the measured critical crack length for this composite is about 32.5 mm. The differences between the cracking loads for the locations of strain gauge-3 and peak load are only 0.11 kN when 1.5% SSWs are introduced, and the critical effective crack length is also about 32.5 mm. The change of cracking interval time, again, explains the crack refinement and bridging effect of SSW on RPC.

3.3 Initial cracking load

Stress concentration in concrete often occurs near original flaws with load increase, causing micro cracks to form and develop in the frontal zones of such flaws. As these micro cracks become saturated, macro cracks are formed. The initial cracking load of SSW reinforced RPC is expressed by F_{ini}, which is determined by the strain gauge reading. The strains on the two sides of the precast crack are collected and marked as strain-1 and strain-4. The load-strain curves are plotted in Fig.6. Due to the inhibiting effect of randomly distributed SSWs on crack initiation, the composite on both sides of

crack tip might is in compression under three-point bending load, e.g. strain-4 in Fig.6

(c). Meanwhile, the strain increases linearly before the initiation of cracks, then, yields

or retracts due to the release of stress and the occurrence of macro cracks. Therefore,

the linear fitting is performed on strain in order to determine the maximum linear strain

point. The initial cracking load is determined by the intersection point between strain

and fitting line, as shown in Fig.6. The average value of the initial cracking load on

both sides of the crack tip is taken as the final value. At the crack length/depth ratio of

0.25, the initial cracking load of RPC without SSW is only 1.0 kN which increase to

1.9 kN and 2.7 kN due to the addition of 1% and 1.5% SSWs. The initial cracking loads

are improved by 91.5% and 183.1% at the crack length/depth ratio of 0.5. The increase

of initial cracking load represents the reduction of original flaws and the uniformity

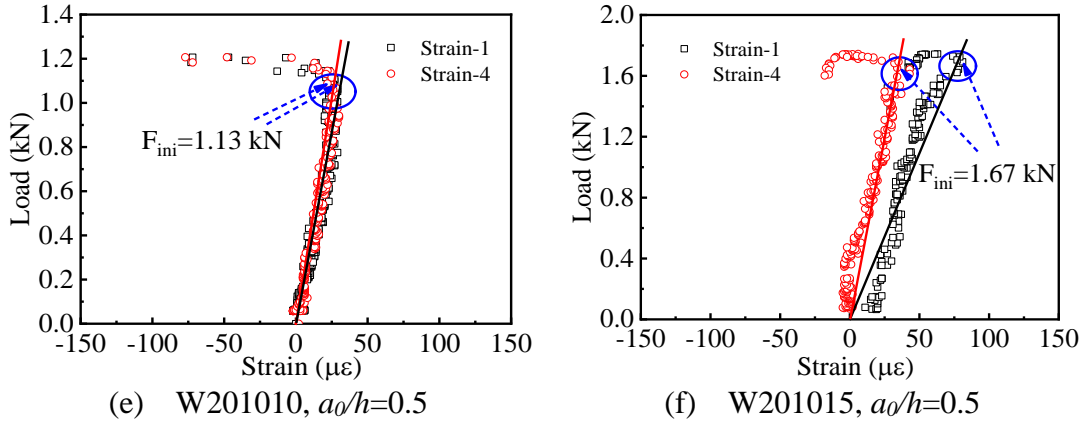improvement of RPC matrix structure.

(a) W0, a_0/h=0.25   (b) W201010, a_0/h=0.25

(c) W201015, a_0/h=0.25   (d) W0, a_0/h=0.5

(e)   W201010, a_0/h=0.5   (f)   W201015, a_0/h=0.5

Fig. 6 Initial cracking load of SSW reinforced RPC

3.4 Fracture toughness calculated with TPFM

The TPFM, proposed by Jenq and Shah [3], is a modified linear elastic fracture mechanics model which turns real crack and micro crack zone into a unified critical effective crack. The fracture criterion is that the effective crack tip opening displacement reaches the critical crack tip opening displacement $CTOD_C$. The fracture toughness K_{IC}^S is calculated at the tip of the effective crack in order to include the nonlinear crack growth prior to peak load. Meanwhile, the unloading compliance used for calculating the critical effective crack length a_c is obtained through at least one loading and unloading process. The calculation of a_c is deduced on the basis of the below Equation (1).

$$E = \frac{6S\alpha V(\alpha)}{C_u th} = \frac{6SP_u}{CMOD_u th}\alpha V(\alpha) \qquad (1)$$

where:

$$V(\alpha) = 0.76 - 2.28\alpha + 3.87\alpha^2 - 2.04\alpha^3 + \frac{0.66}{(1-\alpha)^2} \qquad (2)$$

E is elasticity modulus, the values of elasticity modulus for SSW reinforced RPC can be obtained from refernece [27]; *S* is the span of RPC specimens; $\alpha = a_c/h$, a_c is critical effective crack length; C_u is the unloading compliance; when the load on the descending stage of load-CMOD curve reaches 95% of the peak load, C_u is obtained by assuming that the unloading path returns to the starting point; P_u is the 95% of peak load; $CMOD_u$ refers to the CMOD value corresponding to 95% of peak load on the descending stage of load-CMOD curve; *t* is the width of RPC specimens; *h* is the height of RPC specimens.

The fracture toughness K_{IC}^S is determined by the following Equation (3).

$$K_{IC}^S = 3(P_{max} + 0.5W)\frac{S(\pi a_c)^{1/2}}{2th^2}F(\alpha) \tag{3}$$

where P_{max} is the peak load; $W = W_0 S/h$, W_0 is the dead weight of specimens, which can be ignored here and F(α) is a function of α obtained from Equation (4) below:

$$F(\alpha) = \frac{1.99 - \alpha(1-\alpha)(2.15 - 3.93\alpha + 2.7\alpha^2)}{\pi^{1/2}(1 + 2\alpha)(1-\alpha)^{3/2}} \tag{4}$$

The crtical tip opening dispalcement $CTOD_C$ can be calculated from the following Equation (5).

$$CTOD_C = \frac{6P_{max}Sa_cV(\alpha)}{Eth^2}\left[(1-\beta)^2 + (1.081 - 1.149\alpha)(\beta - \beta^2)\right]^{1/2} \tag{5}$$

where $\beta = a_0/a_c$, a_0 is the intial crack length, a_c is the critical effective crack length.

The normalization parameters of TPFM are tensile strength f_t and brittleness index *Q*, calculated from Equations (6) and (7) below.

$$f_t = \frac{1.4705(K_{IC}^S)^2}{E \times CTOD_C} \tag{6}$$

$$Q = \left(\frac{E \times CTOD_C}{K_{IC}^{S}} \right)^2 \qquad (7)$$

The fracture parameters calculated on the basis of TPFM are shown in Tables 2 and 3. As listed in Tables 2 and 3, the critical effective crack length obtained from TPFM is little affected by SSW volume fraction and is similar with the measured result (as shown in Table 1). Compared with control RPC, the increases of fracture toughness K_{IC}^{S} are determined as 112.3% and 151.7% respectively for RPC reinforced with 1% and 1.5% SSWs at the crack length/depth ratio of 0.25. Considerable increases of 32.1% and 85.2% for crack tip opening displacement $CTOD_C$ are obtained. Meanwhile, the normalization tensile strength f_t and brittleness index Q are improved by 71.0%, 134.0% and 54.6%, 16.0% respectively. At the crack length/depth ratio of 0.5, the fracture toughness K_{IC}^{S} of SSW reinforced RPC increases by 110.3% and 203.4% compared to that of RPC without SSW. The crack tip opening displacement $CTOD_C$ of composites is 55.1% and 113.3% higher than that of control RPC. The normalization tensile strength is enhanced by 102.6% and 194.4%, respectively. The variation of normalization brittleness index at different crack length/depth ratios can be attributed to the multiple cracking and crack refinement characteristics of RPC reinforced with high SSW volume fraction.

Table 2 a_0/h=0.25, TPFM fracture parameters of SSW reinforced RPC

Specimens	E /GPa	$CMOD_{0.95}$ /mm	$F_{un,\,0.95}$ /kN	a_c /mm	K_{IC}^{S} /MPa·m$^{1/2}$	$CTOD_C$ /mm	f_t /MPa	Q /mm
W0	31.0	0.0849	1.29	28.0	2.488	0.0586	5.00	533.21
W201010	43.6	0.1577	2.38	29.7	5.282	0.0774	8.55	824.56
W201015	45.4	0.1565	3.20	28.5	6.263	0.1085	11.71	618.49

Table 3 a_0/h=0.5, TPFM fracture parameters of SSW reinforced RPC

Specimens	E /GPa	$CMOD_{0.95}$ /mm	$F_{un,\,0.95}$ /kN	a_c /mm	K_{IC}^{S} /MPa·m$^{1/2}$	$CTOD_C$ /mm	f_t /MPa	Q /mm
W0	31.0	0.1007	0.57	32.3	2.042	0.0428	4.62	421.90

| W201010 | 43.6 | 0.1553 | 1.15 | 32.5 | 4.294 | 0.0664 | 9.36 | 454.60 |
| W201015 | 45.4 | 0.2135 | 1.67 | 32.5 | 6.196 | 0.0913 | 13.60 | 447.95 |

As the crack length/depth ratio increases, the $K_{IC}{}^{S}$ of RPC composites decreases by 18.2%, 18.7% and 1.1% and the $CTOD_C$ of composites is lowered by 27.0%, 14.2% and 15.9%, respectively. The normalization tensile strength of RPC without SSW is reduced by 7.6%, while 9.5% and 16.2% of increases are obtained for the RPC reinforced with 1% and 1.5% SSWs. This phenomenon illustrates that the toughening effect of high content SSW is more significant with the increase of crack length/depth ratio.

The improvement of $K_{IC}{}^{S}$ and $CTOD_C$ caused by SSWs for RPC is better than that caused by carbon nanotubes, polypropylene fiber and basalt fiber for normal concrete as reported in earlier investigations [35-37], and is comparable to the enhancement effect of 4% volume fraction of steel fiber (with diameter of 0.22 mm) on RPC and 1% volume fraction of hooked-end steel fiber [12,13] on normal concrete. Moreover, the value of $K_{IC}{}^{S}$ for RPC reinforced with 1.0% SSWs is much higher than that for RPC reinforced with 4% steel fiber [13].

3.5 Fracture toughness calculated with DKFM

The DKFM employs initiation fracture toughness K_{IC}^{ini} and unstable fracture toughness K_{IC}^{un} to describe the initial cracking and unstable state of concrete materials [5]. The initiation fracture toughness K_{IC}^{ini} is calculated by initial crack length a_0 and initial crack load P_{ini}, indicating the ability of materials to resist an external load before the generation of cracks. The value of K_{IC}^{ini} can be evaluated by using the following Equation (8).

$$K_{IC}^{ini} = \frac{3P_{ini}S}{2th^2}\sqrt{a_0}\,F(\alpha_0) \tag{8}$$

where $\alpha_0 = a_0/h$; a_0 is the initial crack length of RPC specimens; h is the height of specimens; S is the span of specimens; P_{ini} is the initial cracking load; the expression of $F(\alpha_0)$ is the same as Equation (4). The critical effective crack length a_c can be obtained by Equation (9).

$$a_c = \frac{\left[\gamma^{3/2} + m_1(\beta)\gamma\right]h}{\left[\gamma^2 + m_2(\beta)\gamma^{3/2} + m_3(\beta)\gamma + m_4(\beta)\right]^{3/4}} \tag{9}$$

where

$$\gamma = \frac{CMOD_C\,tE}{6F_{un}}$$

$$m_1(\beta) = \beta\left(0.25 - 0.0505\beta^{1/2} + 0.0033\beta\right)$$

$$m_2(\beta) = \beta^{1/2}\left(1.155 + 0.215\beta^{1/2} - 0.0278\beta\right)$$

$$m_3(\beta) = -1.38 + 1.75\beta$$

$$m_4(\beta) = 0.506 - 1.057\beta + 0.888\beta^2$$

$CMOD_C$ is the crack mouth opening displacement corresponding to peak load; E is the elasticity modulus of composites; t is the width of RPC specimens; h is the height of RPC specimens; $\beta = S/h$ is the span-depth ratio.

The unstable fracture toughness K_{IC}^{un} is determined by critical effective crack length a_c and peak load P_{max}, representing the crack resistance of materials to external

load at critical situation. Therefore, the value of K_{IC}^{un} can be evaluated by inserting a_c and P_{max} into Equation (8) instead of a_0 and P_{ini} respectively.

As shown in Table 4, the critical effective crack length a_c is little affected by the addition of SSW at the crack length/depth ratio of 0.25. The values of a_c are close to the measured results shown in Table 1. The increase of initiation fracture toughness K_{IC}^{ini} reaches 89.2% and 160.0%, and the unstable fracture toughness K_{IC}^{un} is enhanced by 130.8% and 152.4%, respectively due to the addition of 1% and 1.5% SSWs. The improvement of fracture toughness reflects the inhibiting and bridging effect of SSW on the generation and propagation of cracks in RPC.

Table 4 a_0/h=0.25, DKFM fracture parameters of SSW reinforced RPC

Specimens	E /GPa	$CMOD_C$ /mm	F_{ini} /kN	F_{un} /kN	a_c /mm	K_{IC}^{ini} /MPa·m$^{1/2}$	K_{IC}^{un} /MPa·m$^{1/2}$
W0	31.0	0.0619	1.0	1.39	26.3	0.427	2.041
W201010	43.6	0.1153	1.9	2.51	28.2	0.807	4.696
W201015	45.4	0.1080	2.7	3.37	26.5	1.109	5.151

Table 5 a_0/h=0.5, DKFM fracture parameters of SSW reinforced RPC

Specimens	E /GPa	$CMOD_C$ /mm	F_{ini} /kN	F_{un} /kN	a_c /mm	K_{IC}^{ini} /MPa·m$^{1/2}$	K_{IC}^{un} /MPa·m$^{1/2}$
W0	31.0	0.0861	0.59	0.60	31.6	0.487	1.890
W201010	43.6	0.1225	1.13	1.25	31.6	0.940	3.792
W201015	45.4	0.1601	1.67	1.74	31.4	1.389	5.277

Table 5 illustrates that at the crack length/depth ratio of 0.5, the critical effective crack length a_c is also comparable to the measured results shown in Table 1. The initiation fracture toughness K_{IC}^{ini} of SSW reinforced RPC shows an increase of 93.0% and 185.2% and the unstable fracture toughness K_{IC}^{un} grows by 100.6% and 179.2%, respectively. The enhancement effect of SSW on RPC matrix and the bridging effect of SSW on adjacent cracks are not subject to crack length/depth ratio.

The enhancement ratio for K_{IC}^{ini} and K_{IC}^{un} of RPC caused by 1.5% volume fraction of SSW is higher than that caused by the addition of 1.5% steel fibers as reported in reference [38]. Furthermore, compared with previous investigations, K_{IC}^{ini} of SSW reinforced RPC is superior to that of C80 concrete (0.73 MPa·m$^{1/2}$) [39], and the K_{IC}^{un} of the composites exceeds that of polypropylene fiber reinforced concrete (2.18 MPa·m$^{1/2}$) [40], steel fiber reinforced concrete (with diameter of 0.22 mm and volume fraction of 4%, 2.31 MPa·m$^{1/2}$) [13], and carbon nanotube reinforced concrete [41].

3.6 Fracture energy

The fracture energy is defined as the amount of energy to create one unit area of a crack and can be calculated by the following Equation (10) [42]:

$$G_{F-P(\delta)} = \frac{\int P(\delta)d\delta}{(h - a_0)t} \tag{10}$$

where $G_{F-P(\delta)}$ is the fracture energy; δ is the deflection; h is the height of RPC specimens; a_0 is the initial crack length in RPC specimens; t is the width of RPC specimens.

It should be noted that the tail of the descending stage on load-deflection curves is very gentle. It takes a long time for the load dropping to zero in actual test. Generally, the test is stopped as the load drops to a certain value (as shown in Fig.7 (a)), and the value of fracture energy is significantly affected by the tail of load-deflection curve [43]. Elices et al. [44] proposed that the experimental error can be eliminated by including the work of fracture that is not measured due to practical difficulties in capturing the tail part of the load-deflection curves. The relative complete load-deflection curve (as plotted in Fig.7 (b)) can be obtained by fitting and modifying the tail. Then, the fracture

energy can be canculated on the basis of the modified load-deflection curve using Equation (11). The symbols in the equation have the same meaning as above.

$$G_{F-N} = \frac{\int P(\delta)^* d\delta}{(h - a_0)t} \tag{11}$$

(a) Load-deflection curve without tail fitting
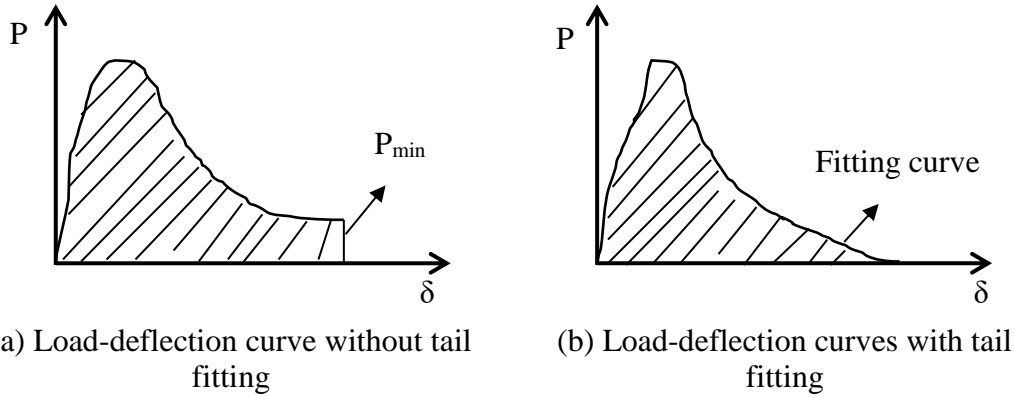
(b) Load-deflection curves with tail fitting

Fig. 7 Typical load-deflection curve for notched three-point bending beam [43]

In order to avoid the tail treatment influence on fracture energy, the tail of load-deflection curves is extended according to exponential equation in this paper, as demonstrated in Fig.8. The fracture energy of SSW reinforced RPC obtained by load-deflection curves with and without tail fitting is listed in Table 6.

(a) a_0/h=0.25

(b) a_0/h=0.5
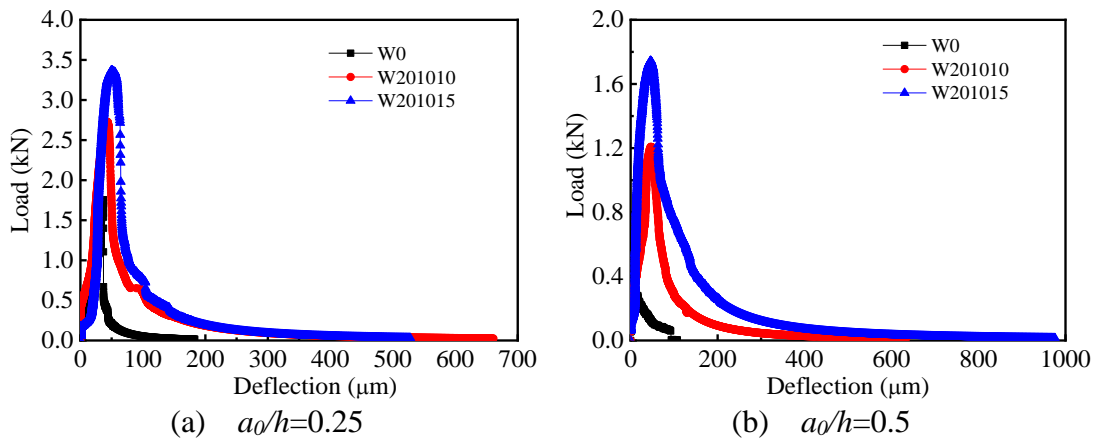
Fig. 8 Load-deflection curves of SSW reinforced RPC with tail fitting

Table 6 Fracture energy of SSW reinforced RPC

Specimens	$G_{F-P(\delta)}$ (Standard deviation)	Tail fitting equation	G_{F-N} /J/m²	(G_{F-N}-	P_{min}/P_c /%

		/J/m²			$G_{F-P(\delta)})/$ $G_{F-P(\delta)}$ /%	
a_0/h=0.25	W0	32.02 (2.80)	-	32.02	-	-
	W201010	106.89 (11.26)	y=1206.39767x-1.65811	152.89	43.0	10.5
	W201015	173.07 (10.34)	y=4787.56857x-1.91069	183.45	6.0	7.0
a_0/h=0.5	W0	19.70 (0.70)	-	19.70	-	-
	W201010	85.58 (9.26)	y=843.79299x-1.72037	118.39	38.3	14.4
	W201015	220.06 (10.60)	y=4479.37484x-1.84429	253.19	15.1	12.8

As shown in Table 6, the fracture energy $G_{F-P(\delta)}$ of SSW reinforced RPC calculated on the basis of Equation (10) displays a notable increase compared to that of control RPC. The inclusion of 1.0% and 1.5% SSWs leads to 233.8% and 440.5% increase in fracture energy at the crack length/depth ratio of 0.25, and the increments can reach 334.4% and 1017.1%, respectively, at the crack length/depth ratio of 0.5. The fracture energy of RPC reinforced with 1.5% SSWs increases with the increasing crack length/depth ratio. The fracture energy G_{F-N} of SSW reinforced RPC calculated on the basis of Equation (11) exhibits higher value than that calculated on the basis of Equation (10). The error between G_{F-N} and $G_{F-P(\delta)}$ is more than 15% and even as high as 43% because that the ratio of cut-off load P_{min} to peak load P_c on load-deflection curve is higher than 10%. The percentage difference between G_{F-N} and $G_{F-P(\delta)}$ falls within the margin of error when the ratio of cut-off load P_{min} to peak load P_c is lower than 10%. It can be concluded that whether the load-deflection curve is tail-fitted or not has no influence on the relationship between fracture energy and SSW volume fraction. However, the cut-off load P_{min} on load-displacement curve should be controlled within 10% of peak load in order to eliminate the test error as much as possible. The increment of fracture energy caused by 1% SSWs is superior to that caused by 0.5% steel fiber in

existing study [7, 9], although the fracture energy values of SSW reinforced RPC in this paper are lower than that of hooked-end steel fiber reinforced concrete [12, 13].

3.7 Cracking pattern

The cracking patterns of SSW reinforced RPC at failure state are demonstrated in Figs.9 and 10. It can be seen from Figs. 9 and 10 that the cracking patterns of the composites are tortuous and blunt cracks as the crack resistance zone is formed by SSWs and RPC matrix together. The development trace of crack bypassing fine aggregate can be observed on the RPC specimens without SSW (as shown in Fig. 9(a) and Fig.10 (a)). The failure cracks of composites become narrow, short and tortuous due to the increase of SSW volume fraction, as shown in Fig. 9 (b), (c) and Fig. 10 (b), (c). The blunt and tortuous cracks reduce the stress concentration at notch tip. The specimens of SSW reinforced RPC are not completely disconnected when failure occurs, and the bridging SSWs can be clearly observed. The failure surface of the composites is rather unsmooth due to the resistance effect of SSWs. The cracking pattern change law of SSW reinforced RPC is consistent with the test results of fracture toughness and fracture energy.
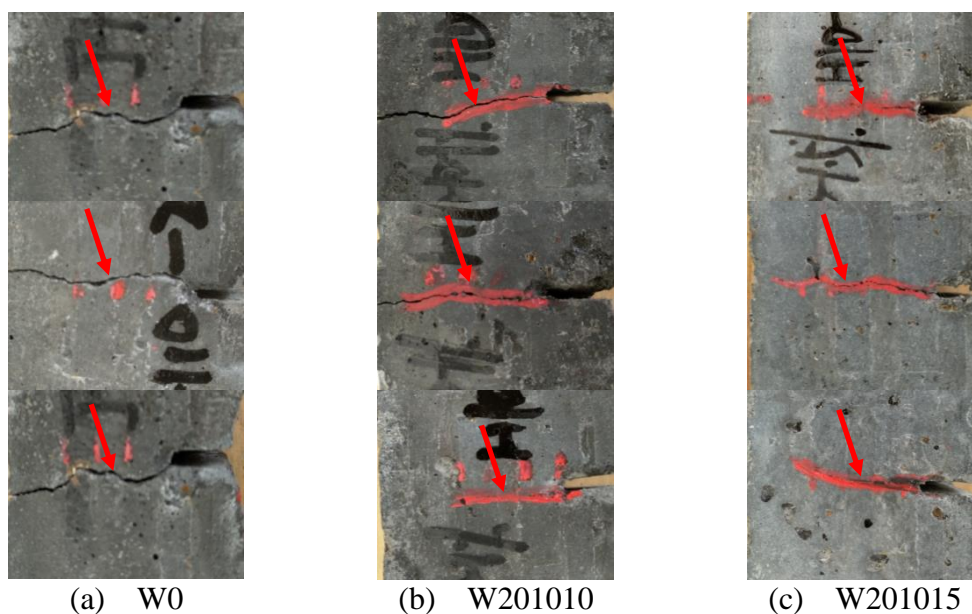

(a) W0　　　　　　　　(b) W201010　　　　　　　　(c) W201015

Fig. 9 a_0/h=0.25,   cracking patterns of SSW reinforced RPC under three-point bending load

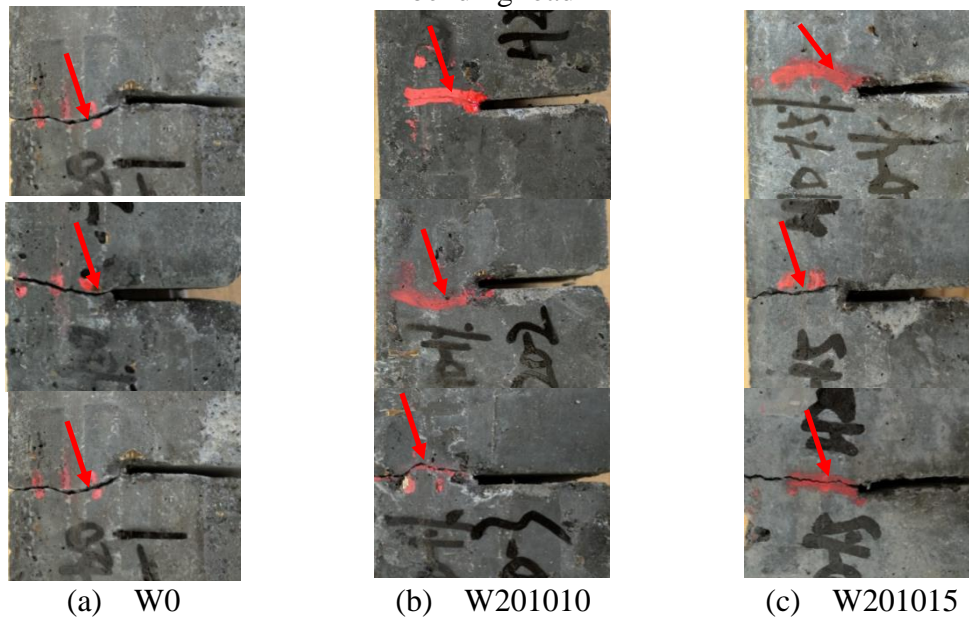(a)   W0   (b)   W201010   (c)   W201015

Fig. 10 a_0/h=0.5, cracking patterns of SSW reinforced RPC under three-point bending load

4 Four-point shearing fracture behaviors

The four-point shearing beams are employed to study the mixed mode I-II fracuture characteristics of SSW reinforced RPC. The shear force Q can be calculated using the following Equations (12) and (13) [45].

$$F_1/F_2 \ = \ (S - c)/c \tag{12}$$

$$Q \ = \ F_1 - F_2 \ = \ \frac{S - 2c}{S} \, F \tag{13}$$

where F is the applied load on beam specimens; F_1 represens the load at the near loading point; F_2 represens the load at the far loading point; S is the distance between the far loading point and the near loading point; c is the distance between the near loading point and the center line of initial precast crack. The stress intensity factor K_{I-II} for mixed mode I-II fracture can be calculated by the following Equation (14) [45].

$$K_{I\text{-}II} = \frac{Q}{t\sqrt{h}}\ f(a_0/h) \tag{14}$$

$$f(a_0/h) = \left[1.442 - 5.08\left(\frac{a_0}{h} - 0.507\right)^2\right] \times sec\ \frac{\pi a_0}{2h}\ \sqrt{sin\ \frac{\pi a_0}{h}} \tag{15}$$

where t is the width of RPC specimens; h is the height of RPC specimens; a_0 is the initial crack length; $f(a_0/h)$ is dimensionless stress intensity factor, which is related to cracking pattern and initial crack length/depth ratio. The RPC specimens are in failure state when the concentrated load F reaches the maximum value F_m. The maximum shear force Q_m can be obtained according to Equation (13). The stress intensity factor under concentrated load F_m is the fracture toughness $K_{I\text{-}IIc}$ obtained from:

$$K_{I\text{-}IIc} = \frac{Q_m}{t\sqrt{h}}\ f(a_0/h) \tag{16}$$

4.1 Load-CMOD curves

The load-CMOD curves of SSW reinforced RPC under four-point shearing load are plotted in Fig.11. It can be seen from Fig.11 that, the nonlinear ascending stage of load-CMOD curves becomes more and more obvious with the increasing SSW volume fraction. At this stage, the generation and propagation of cracks are hindered by SSW disordered network. When the volume fraction of SSW is 1.5%, the slope of linear ascending stage has a remarkable decline. Moreover, there is a stationary stage for load-CMOD curve before peak load. Compared with RPC without SSW, the peak CMOD ($CMOD_C$) enhancement of RPC reinforced with 1.5% SSWs reaches up to 625.0% at crack length/depth ratio of 0.25. The $CMOD_C$ of RPC reinforced with 1% and 1.5% SSWs is improved by 68.0% and 232.0% respectively at crack length/depth ratio of 0.5.

With the increase of crack length/depth ratio, the $CMOD_C$ of RPC reinforced with 1.5% SSWs is reduced by 28.4%. This is because that the incorporation of 1.5% SSWs enables the occurrence of pure shear crack.
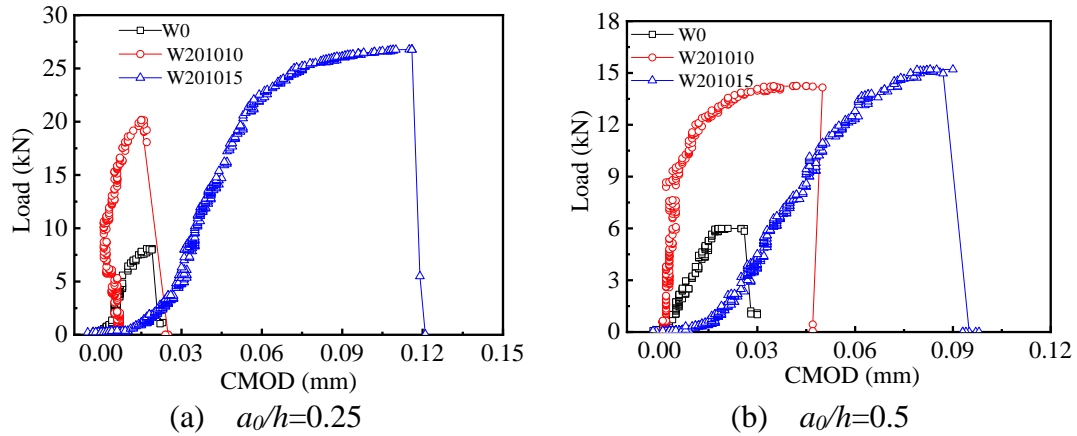

(a) a_0/h=0.25   (b) a_0/h=0.5

Fig. 11 Load-CMOD curves of SSW reinforced RPC under four-point shearing load

4.2 Shear force and mixed mode I-II fracture toughness

As demonstrated in Fig.12 (a), the failure shear force of SSW reinforced RPC significantly exceeds that of RPC without SSW. Increments of 123.9% and 177.4% are obtained for shear force of RPC reinforced with 1% and 1.5% SSWs at the crack length/depth ratio of 0.25, and the shear force increments for composites are 119.4% and 137.1% respectively at the crack length/depth ratio of 0.5. The shear force decreases with the increase of crack length/depth ratio.

(a) Shear force   (b) Fracture toughness
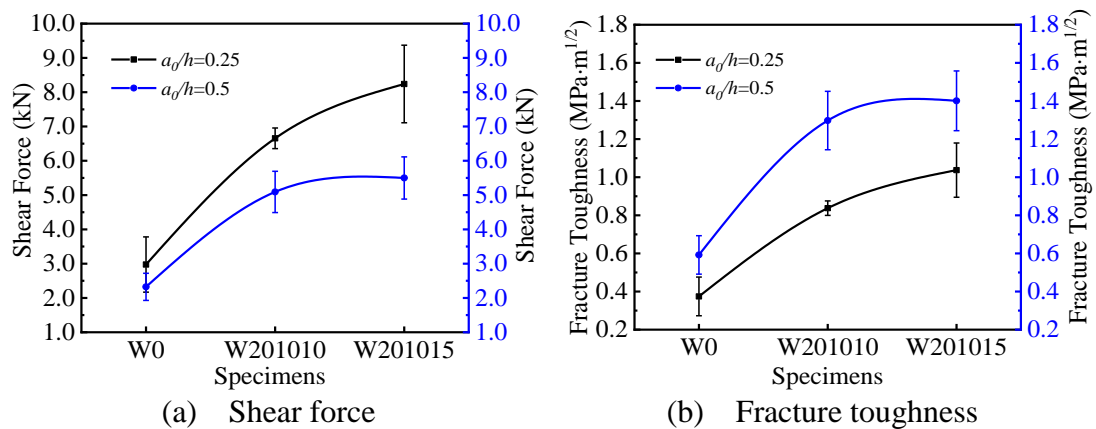
Fig. 12 Shear force and fracture toughness of SSW reinforced RPC

Fig.12 (b) manifests that the mixed mode I-II fracture toughness of RPC reinforced with 1% and 1.5% SSWs is increased by 123.8% and 177.1% compared to that of RPC without SSW at the crack depth ratio of 0.25, and the growth rates of 118.6% and 137.3% are achieved at the crack length/depth ratio of 0.5. The mixed mode I-II fracture toughness of the composites is proportional to shear force, and they are improved by 59.5%, 54.8% and 35.0% respectively as the crack length/depth ratio increases from 0.25 to 0.5. The fracture toughness values of SSW reinforced RPC are larger than that for concrete and rock obtained by Mirsayar et al. [46] and Pirmohammad et al. [19].

4.3 Cracking pattern

There are four types of cracking pattern for SSW reinforced RPC under four-point shearing load as explained below.

(1) The specimens are fractured along an oblique straight crack running from the precast crack tip to the near loading point, as shown in Fig.13 (a). These are typical mixed mode I-II fracture cracks which bear both bending moment and shear force. The cracks are prone to occur when the distance between the two near loading points is far away.

(2) There are two cracks in the failure specimens: one is an oblique crack running from the precast crack tip to the near loading point, and the other is a crack vertically upward along the near loading point, as exhibited in Fig.13 (b). This kind of failure occurs at the crack length/depth ratio of 0.25. The oblique crack belongs to I-II mixed mode type and the vertical crack is caused by stress concentration.

(3) Two cracks vertically upward along the near loading point are generated because of stress concentration, as demonstrated in Fig.13 (c). Such failure also occurs only at the crack length/depth ratio of 0.25.

(4) Fig.13 (d) shows that two cracks are produced in the failure specimens at the crack length/depth ratio of 0.5: one is an oblique crack running from the precast crack tip to the near loading point, and the other is a nearly vertical crack along the direction of precast crack. The oblique crack belongs to I-II mixed mode type and the vertical crack is pure shear type.

| W0, a_0/h=0.25 | W0, a_0/h=0.5 | W201015, a_0/h=0.5 |

(a)　The first kind of cracks

| W0, a_0/h=0.25 | W201010, a_0/h=0.25 | W201015, a_0/h=0.25 |

(b)　The second kind of cracks

| W201010, a_0/h=0.25 | W201015, a_0/h=0.25 |

(c)　The third kind of cracks

| W0, a_0/h=0.5 | W201010, a_0/h=0.5 | W201015, a_0/h=0.5 |

(d)　The forth kind of cracks
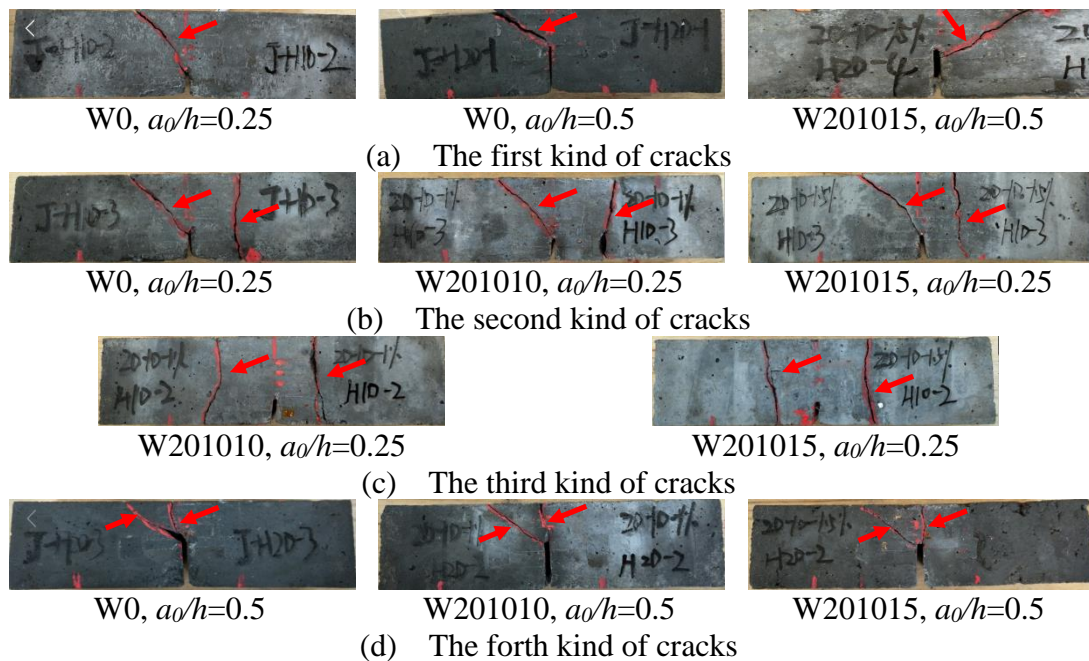
Fig. 13 Cracking patterns of SSW reinforced RPC under four-point shearing load

It can be concluded that the failure cracks of SSW reinforced RPC under four-point shearing load are mainly I-II mixed mode type and stress concentration type at the crack length/depth ratio of 0.25, while the cracks are mainly I-II mixed mode type and shear type at the crack length/depth ratio of 0.5. Fig.13 also shows that the angle between mixed mode I-II crack and precast crack extension line decreases and the propagation of stress concentration crack becomes more tortuous with the increase of

SSW volume fraction. The shear cracks at the upper end of the precast crack first slope toward the near loading point and then turn to the parallel direction of load. The transverse shear crack parallel to load direction occurs in the specimens of RPC reinforced with 1.5% SSWs. This can be attribute to that the incorporation of high volume fraction of SSW enhances the tensile strength of RPC and limits the development direction of initial crack.

4.4 Initial cracking load

The analysis of initial cracking load is performed on the SSW reinforced RPC specimens with two failure cracks. The load-strain curves of the composites are drawn in Fig.14. It can be observed from Fig.14 that the strain increases with the increasing load, while the growth rate of strain is accelerated or hysteretic after the occurrence of initial crack.

(a)　W0, a_0/h=0.25　　　　　　　(b)　W201010, a_0/h=0.25

(c)　W201015, a_0/h=0.25　　　　　　(d)　W, a_0/h=0.5

(e) W201010, a_0/h=0.5　　　　　(f) W201015, a_0/h=0.5
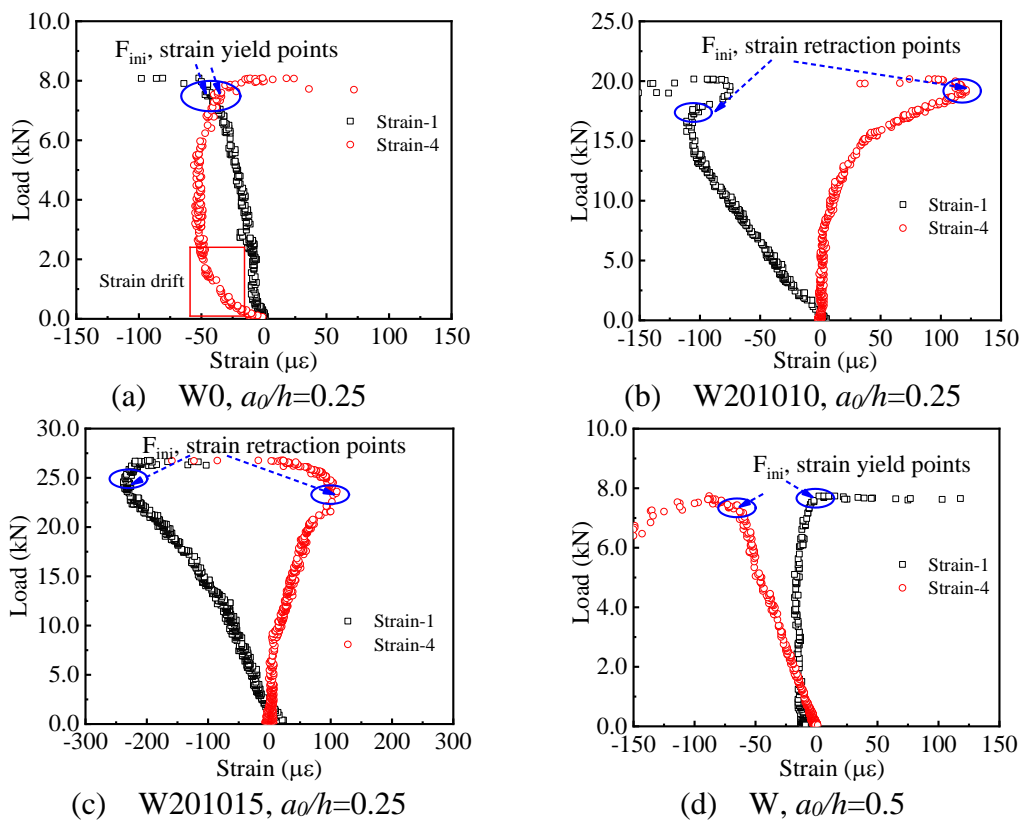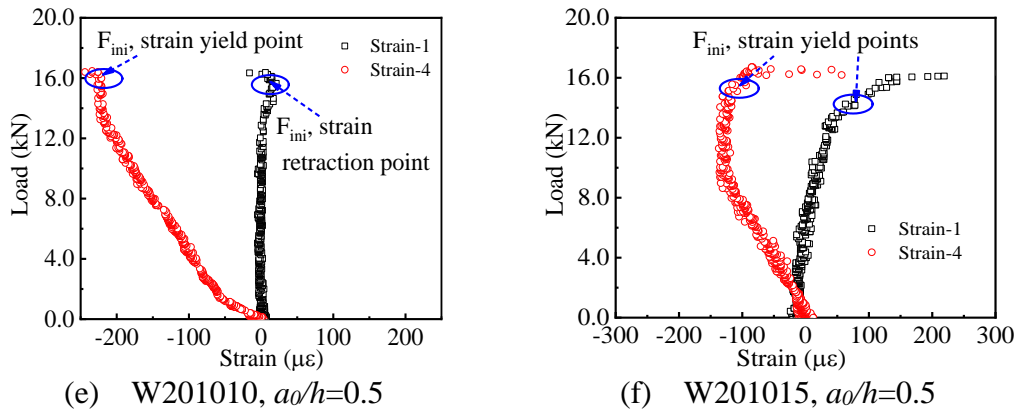
Fig.14　Four-point shearing initial cracking load of SSW reinforced RPC

Table 7 Initial cracking load of SSW reinforced RPC under four-point shearing load

	a_0/h=0.25				a_0/h=0.5		
Specimens	Initial cracking load F_{ini}, kN	Peak load F_{un}, kN	F_{ini}/F_{un}	Specimens	Initial cracking load F_{ini}, kN	Peak load F_{un}, kN	F_{ini}/F_{un}
W0	7.6	8.1	0.941	W0	7.5	7.7	0.974
W201010	19.0	20.2	0.940	W201010	16.0	16.5	0.970
W201015	24.5	26.7	0.915	W201015	15.9	16.7	0.952

As shown in Fig.14, the strain on both sides of precast crack is complex under four-point shearing load because of the inhibiting effect of SSW on crack initiation. However, whether the composite on both sides of precast crack is in tension or compression, strains will yield or retract due to the initiation of cracks. Therefore, the load corresponding to yield strain point or retraction strain point is defined as the initial cracking load. The initial cracking load of SSW reinforced RPC is summarized in Table 7. As demonstrated in Table 7, the ratio of initial cracking load F_{ini} to peak load F_{un} is reduced by the increasing volume fraction of SSW. This corresponds to the phenomenon that the load-CMOD curves of the composites possess significant nonlinear ascending stage. The initial cracking loads of RPC reinforced with 1% and 1.5% SSWs are 150.0% and 222.3% higher than that of RPC without SSW at the crack length/depth ratio of 0.25. The increments of initial cracking load are calculated to be 113.3% and 112.0% at the crack length/depth ratio of 0.5.

The increase of initial cracking load validates the enhancement effect of SSW on RPC matrix. Meanwhile, the decrease of the ratio between initial cracking load and peak load proves the inhibiting and bridging effect of SSW on the generation and propagation of cracks.

5 Fracture self-sensing behaviors

5.1 Under three-point bending

At the crack length/depth ratio of 0.25, the fracture self-sensing properties of SSW reinforced RPC obtained by three-point bending test are plotted in Fig.15. The variation of FCR with load is the same as that of strain, CMOD and deflection with load, which can be divided into three stages: stationary stage, rapid rising stage and sharp rising stage.

It can be seen from Fig.15 (a) that the strain, CMOD, deflection and FCR of control RPC are in stationary stage as the load is smaller than 0.43 kN. And then, RPC matrix enters into crack initiation stage. The corresponding strain, CMOD, deflection and FCR are in the stage of rapid rising. However, the growth rate of strain and deflection is much higher than that of CMOD and FCR. The strain, CMOD, deflection and FCR are 3207 με, 0.06 mm, 20.1 μm and 0.12% respectively at the peak load of 1.36 kN. After that, the strain, CMOD, deflection and FCR enter into sharp rising stage as the load decreases. When the load drops to 1.33 kN, the strain reaches the limit value of 4584 με and cracks have passed through the location of strain gauge-2. The CMOD, deflection and FCR are 0.38 mm, 32.7 μm and 1.04% respectively as the load drops to 0.3 kN. This phenomenon indicates that FCR of RPC without SSW is mainly determined by CMOD. Fig.15 (b) shows that the strain, CMOD, deflection and FCR of RPC reinforced with 1% SSWs are in stationary stage as the load is smaller than 1.19 kN. And then, the strain, CMOD and deflection go into rapid rising stage with the

cracking of RPC matrix. The strain firstly advances into sharp rising stage due to the propagation of cracks. The limit value of strain is 3931 µε when the load is 2.34 kN. The corresponding deflection and CMOD move onto sharp rising stage and the FCR steps into rapid rising stage. The deflection, CMOD and FCR are 101.2 µm, 0.4 mm and 6.2% respectively at the peak load of 2.7 kN. Meanwhile, the FCR has been in the stage of sharp rising because of the convergence of cracks. When the load drops to 0.44 kN, the deflection, CMOD and FCR are 0.89 mm, 148.6 µm and 13.6% respectively.

(a) W0

(b) W201010

(c) W201015
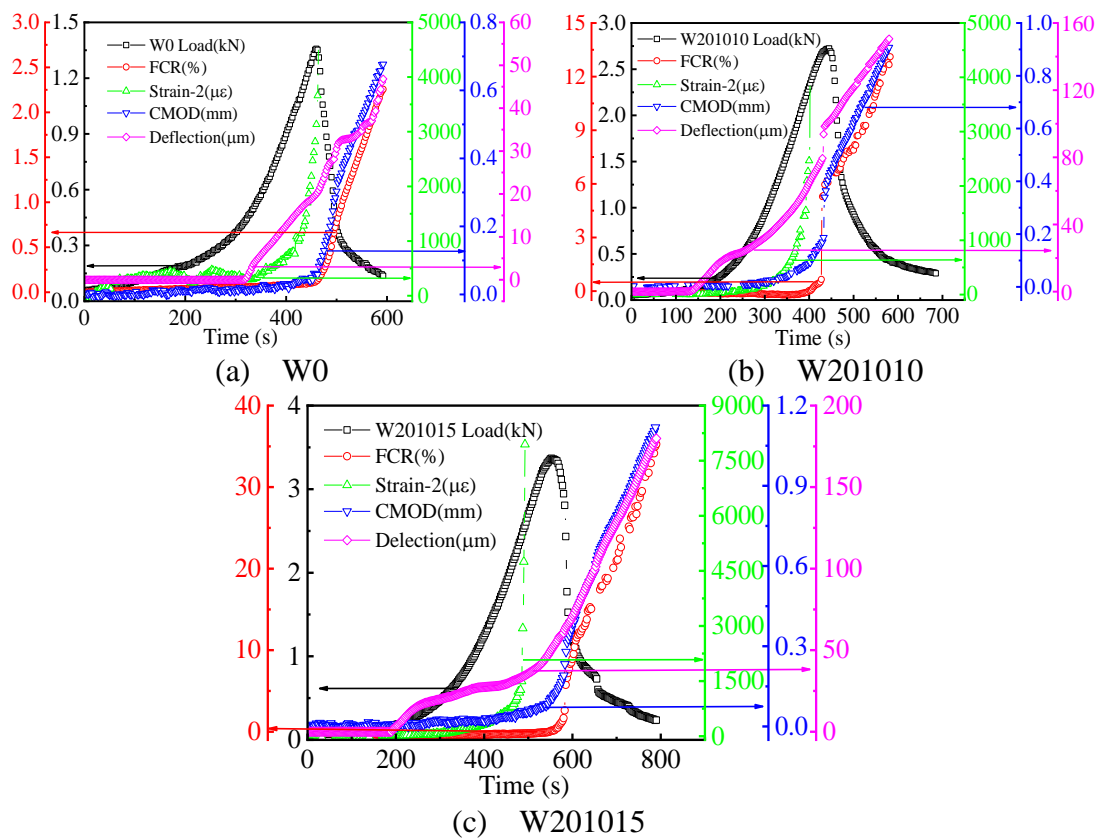
Fig. 15 a_0/h=0.25, three-point bending fracture sensibility of SSW reinforced RPC

As displayed in Fig.15 (c), the strain, CMOD and deflection of RPC reinforced with 1.5% SSWs begin to rise rapidly when the load is 2.48 kN. The strain reaches the extreme value of 7944 µε at a load of 2.56 kN. The FCR steps into rapid rising stage while the CMOD and deflection enter into sharp rising stage after peak load of 3.4 kN.

The corresponding values of CMOD, deflection and FCR are 0.10 mm, 50.4 µm and 0.14% respectively. Due to the rupture of SSWs, the FCR of the composite goes into sharp rising stage as the load drops to 2.81 kN. The CMOD, deflection and FCR are 0.98mm, 157.8 µm and 28.7% respectively as the load drops to 0.3 kN.

At the crack length/depth ratio of 0.5, the fracture self-sensing properties of SSW reinforced RPC obtained by three-point bending test are demonstrated in Fig.16. As can be seen from Fig.16, the variation of strain, CMOD, deflection and FCR of the composites still includes three stages: stationary stage, rapid rising stage and sharp rising stage. It is known from Fig.16 (a) that the strain, CMOD, deflection and FCR of control RPC develop from stationary stage into rapid rising stage as the load is larger than 0.4 kN. The values of strain, CMOD, deflection and FCR are 728 µε, 0.09 mm, 45 µm and 0.02% respectively at peak load of 0.8 kN. And then, the strain, CMOD, deflection and FCR enter into sharp rising stage with the unloading process because of the unstable propagation and convergence of cracks. The strain reaches the limit value of 3200 µε as the load drops to 0.33 kN. Even if the load drops to 0.19 kN, the corresponding FCR of control RPC is only 0.19%.

(a)　W0 　　　　　　　　　(b)　W201010
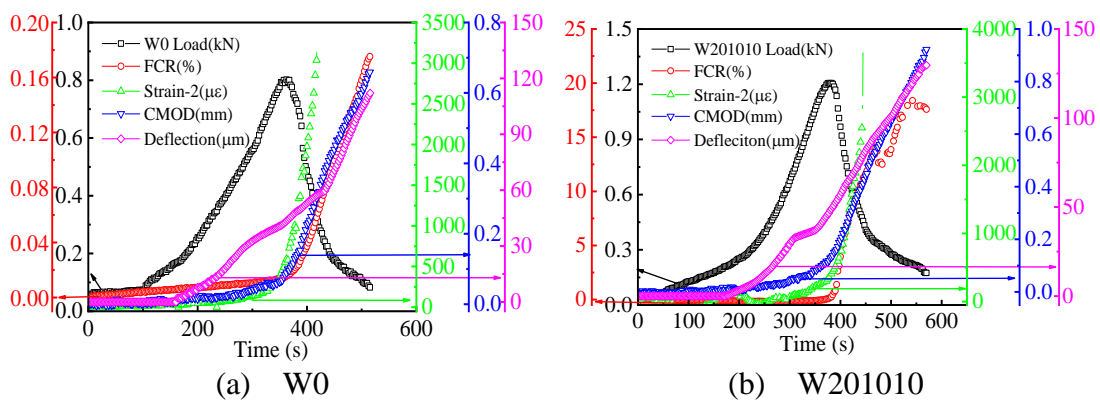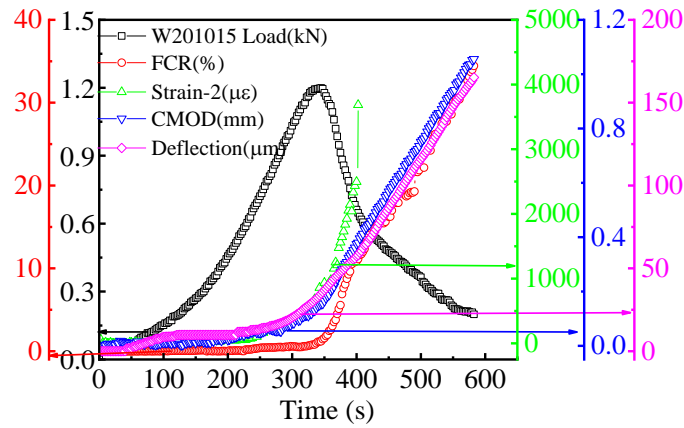
(c) W201015

Fig. 16 *a₀/h*=0.5, three-point bending fracture sensibility of SSW reinforced RPC

As shown in Fig.16 (b), the rapid growth of strain, CMOD, deflection and FCR of RPC reinforced with 1.0% SSWs occurs at the load of 0.6 kN. The values of strain, CMOD, deflection and FCR are 408 με, 0.13 mm, 49 μm and 0.25% respectively at the peak load of 1.2 kN. As the load decreases, the strain, CMOD, deflection and FCR enter into sharp rising stage, and the cracks extend rapidly although hindered by SSWs. The strain gauge-2 has failed as the load decreases to 0.46 kN. When the load drops to 0.19 kN, the CMOD, deflection and FCR are 0.92 mm, 129.6 m and 17.6%, respectively. Fig.16 (c) demonstrates that the strain, CMOD, deflection and FCR of RPC reinforced with 1.5% SSWs go into rapid rising stage at the load of 0.76 kN. When the load reaches the peak value of 1.2 kN, the strain, CMOD, deflection and FCR are 676 με, 0.15 mm, 34 μm and 1.2% respectively. Then, the strain, CMOD, deflection and FCR develop into sharp rising stage with the process of unloading. The strain gauge-2 fails as the load drops to 0.65 kN. When the load drops to 0.19 kN, the CMOD, deflection and FCR are 1.06 mm, 165.7 μm and 34.4%, respectively.

It is summarized that the change rules of strain, CMOD, deflection and FCR versus load for SSW reinforced RPC are the same. The development of strain, CMOD and

deflection can be diagnosed and monitored by the change of electric resistivity. The FCR is mainly dominated by the opening width of cracks at the stage of rapid rising, and then the FCR steps into sharp rising stage as SSWs are ruptured. The ultimate FCR of SSW reinforced RPC far exceeds that of RPC without SSW due to the disconnection of conductive pathway.

5.2 Under four-point shearing

It can be seen from Fig.17 (a) that at the crack length/depth ratio of 0.25, the CMOD of RPC without SSW show a rapid rising trend while the strain show a rapid declining trend at the load of 5.8 kN. The specimens of control RPC have been in cracking state. The FCR of control RPC grows with loading time due to polarization. The CMOD, strain and FCR increase sharply after the load reaches the peak value of 6.95 kN. Then, the load drops instantaneously and the specimens fall in failure state. The RPC without SSW does not have the self-sensing ability to four-point shearing load.
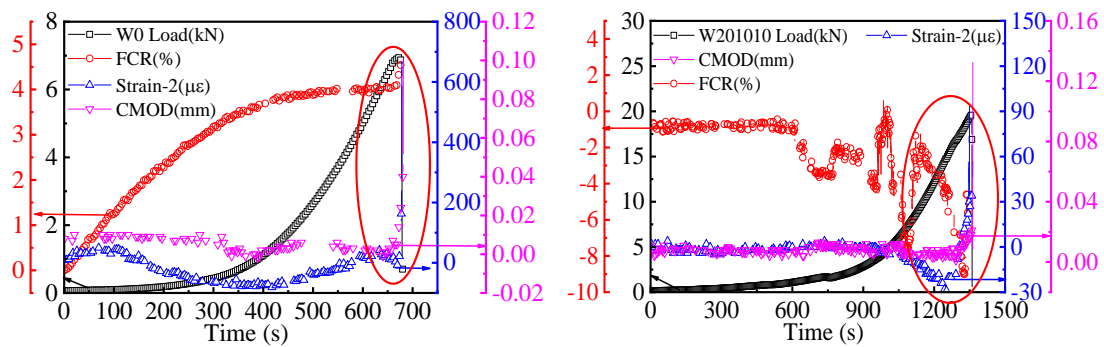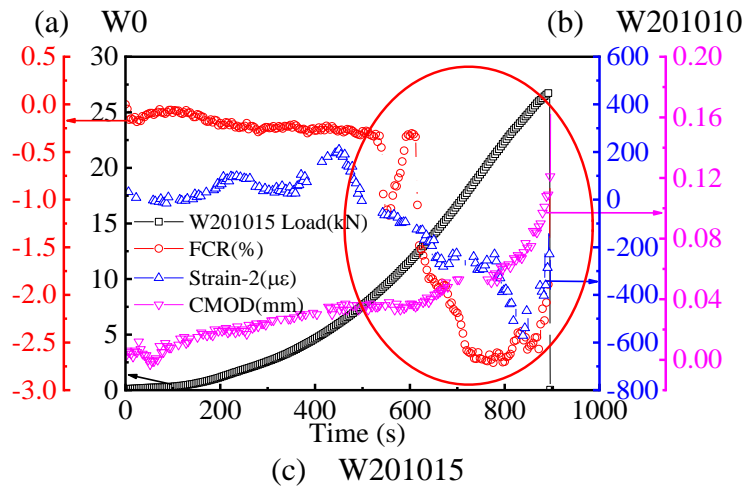
Fig. 17 a_0/h=0.25, four-point shearing fracture sensibility of SSW reinforced RPC

Fig.17 (b) shows that the FCR of RPC reinforced with 1% SSWs fluctuates up and down after the load reaches 1.05 kN. Then, it steps into rapid declining stage and the strain begins to decrease due to the crack initiation of the composite. After that, the FCR goes into sharp declining stage, the strain reaches the minimum value, and the CMOD enters into rapid rising stage because that the specimens have begun to show macro cracks. The FCR reaches the minimum value when the load is 18.3 kN. The conductive pathway is destroyed and the FCR begins to increase with the propagation of cracks. The corresponding CMOD, strain and FCR are 0.011 mm, 32 με and 6.58% respectively at the peak load of 19.6 kN. Fig.17 (c) demonstrates that the FCR and strain of RPC reinforced with 1.5% SSWs are in rapid declining stage, and the CMOD begins to increase rapidly when the load is 8.2 kN. The specimens begin to crack from the precast position. The strain achieves the minimum value of 593 με and then increases when the load is 24.2 kN. This can be attributed to the occurrence of macro cracks and the corresponding FCR is in the rapid rising stage. The FCR, strain and CMOD go into sharp rising stage after the peak load of 26.8 kN.
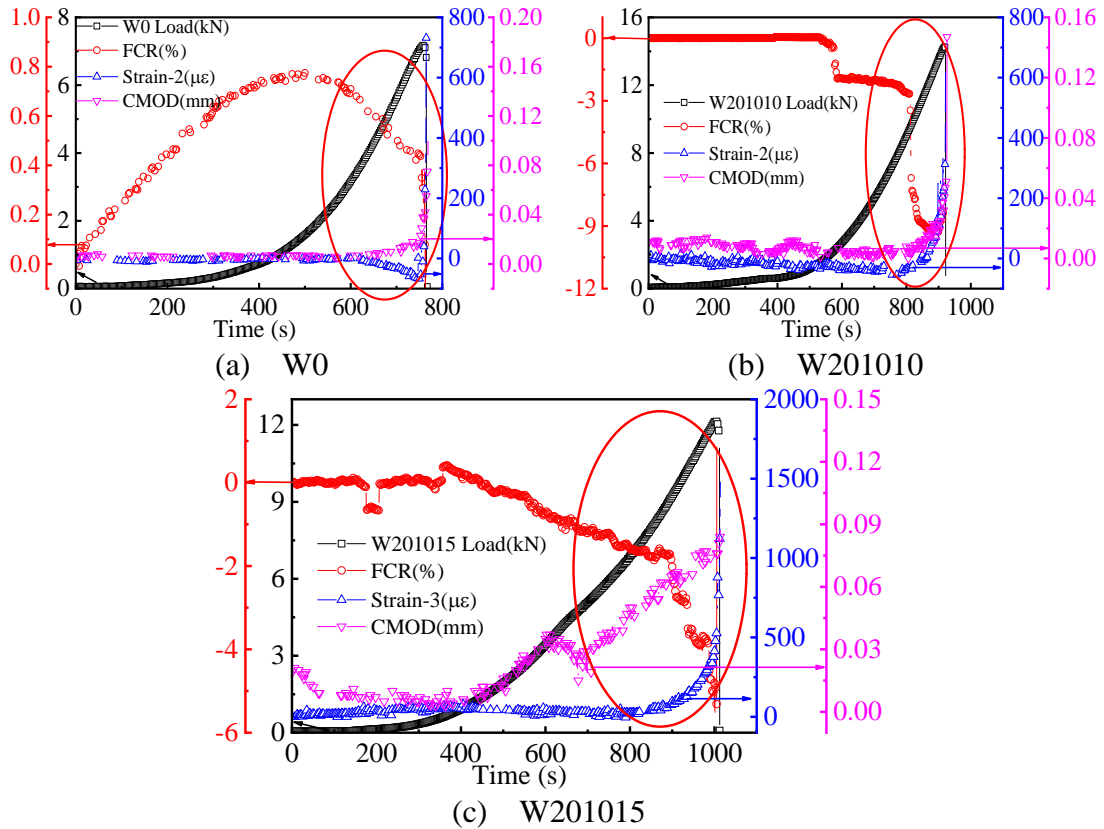
(a) W0

(b) W201010

(c) W201015

Fig. 18 a_0/h=0.5, four-point shearing fracture sensibility of SSW reinforced RPC

At the crack length/depth ratio of 0.5, the FCR of RPC without SSW increases with time because of polarization, as shown in Fig.18 (a). The FCR and strain begin to decrease at the load of 2.2 kN. The FCR reaches the minimum value of 0.44% when the peak load is 7.2 kN. Then, the load drops instantaneously and the specimens are in failure state. Fig.18 (b) displays that when the load is 9.4 kN, the FCR of RPC reinforced with 1% SSWs is in rapid declining stage. The strain and CMOD turn into rapid rising stage because of the emergence of initial cracks. The minimum value of FCR is obtained as the load reaches 14.1 kN, and then the FCR turns to increase due to the appearance of macro cracks. The FCR, strain and CMOD go into sharp rising stage with the load decrease. Fig.18 (c) shows that the FCR of RPC reinforced with 1.5% SSWs is in rapid declining stage while the strain is in rapid rising stage at the load of

9.2 kN. Then, the FCR increases with macro cracks appear. The FCR, strain and CMOD step into sharp rising stage after the peak load of 12.2 kN.

It can be concluded that the variation of FCR can be used for sensing the generation and propagation of cracks in SSW reinforced RPC. The FCR begins to decrease when the initial crack occurs, and it enters into rapid development stage after the appearance of macro cracks. After that, the SSWs are gradually ruptured and the FCR is in sharp rising stage.

6 Fracture and self-sensing mechanisms

The fracture and self-sensing mechanisms of SSW reinforced RPC are explained through analyzing the fracture process zone (FPZ) at the upper end of the precast crack, as shown in Fig.19. The development of FPZ includes three different stages: crack initiation, stable crack propagation and unstable crack propagation.

As demonstrated in Fig.19 (a), the SSWs and RPC matrix work together to form crack resistance zone in SSW reinforced RPC. Owing to the high aspect ratio and large specific surface area of SSW, lots of hydration products gather on the surface of SSW and the original flaws of RPC are reduced, leading to refined grains, homogenous structures, and excellent interfacial transition zone performance of the composites. Therefore, the cracking resistance of the composites is improved, the initial cracking load is enhanced, and the linear ascending stage of load-deflection and load-CMOD curves is prolonged, which eventually increases the fracture toughness and fracture energy. At this stage, the FCR of the composites is in stationary stage and has no obvious change. Fig.19 (b) manifests that the stress concentration leads to the generation of micro cracks, and the saturation of micro cracks results in the formation of macro cracks. The load-deflection and load-CMOD curves of SSW reinforced RPC develop into non-linear ascending stage. The SSWs can relieve the stress concentration

on the tip of micro cracks, and prevent the generation and propagation of macro cracks. Then, the SSWs bridge adjacent macro cracks and the tensile stress is shared by SSWs and RPC matrix together. When all tensile stress is transferred to SSWs, the load-deflection and load-CMOD curves appear a yield stage before peak load. During this process, the FCR of the composites is in rapid development stage which is mainly affected by the opening of crack mouth and the increase of mid-span deflection. The emergence of initial cracks can be detected by variation inflection point of FCR due to the change of conductive pathway under loading [47, 48]. Fig.19 (c) illustrates that the SSWs are gradually ruptured with the propagation of macro cracks. The load-deflection and load-CMOD curves of SSW reinforced RPC present relative slow descending stage. The FCR of the composites is in sharp rising stage due to the rupture of SSWs. The failure process of SSW reinforced RPC can be detected by the change of FCR.
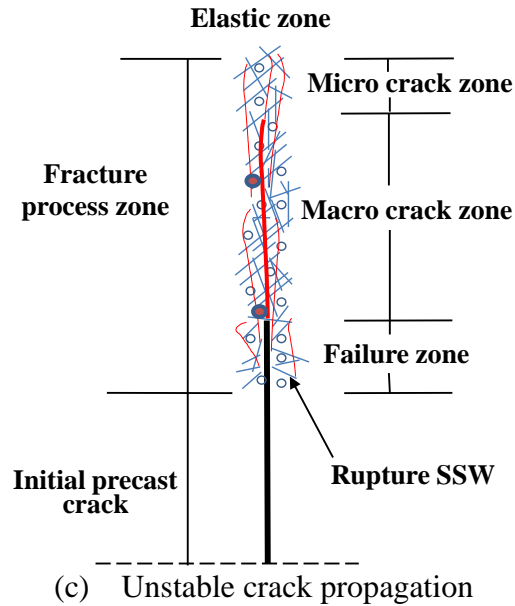

(a) Crack initiation (b) Stable crack propagation

(c) Unstable crack propagation
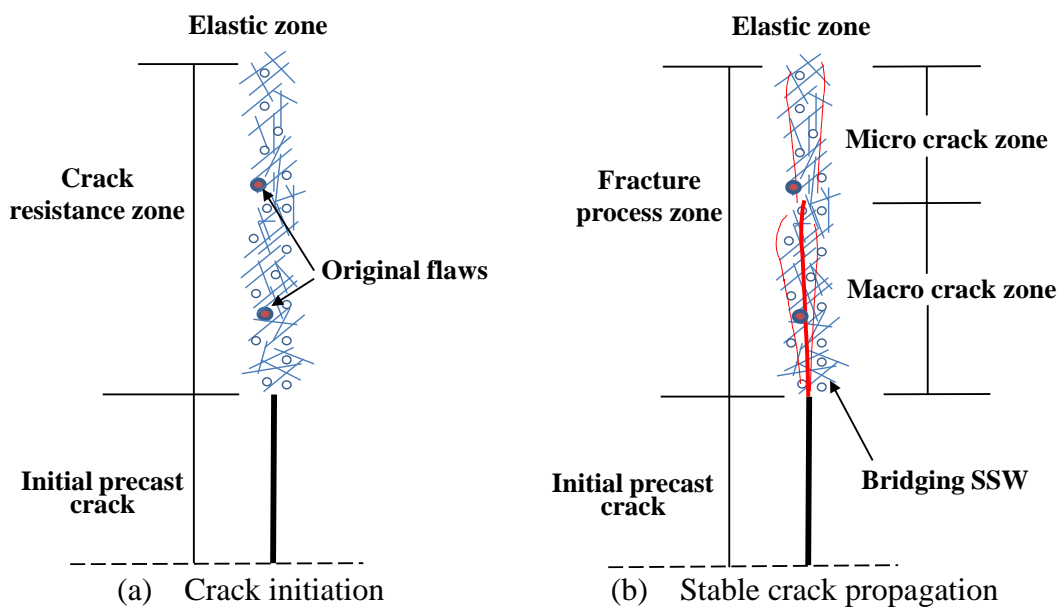
Fig. 19   Fracture and self-sensing mechanisms of SSW reinforced RPC

7 Conclusions

Super-fine stainless wire (SSW) reinforced reactive powder concrete (RPC) presents high mechanical performances and multi-functional properties due to the excellent characteristics of SSW such as micron scale diameter, high aspect ratio and large specific surface area. In addition, the SSWs and RPC matrix work together to form crack resistance zone in concrete structures. Therefore, the fracture characteristics and self-sensing ability of SSW reinforced RPC were investigated under three-point bending and four-point shearing load in this paper.

The load-deflection and load-CMOD curves of SSW reinforced RPC possess long linear elastic stage, significant non-linear ascending stage and slow descending stage under three-point bending load. The crack propagation resistance of the composites is improved and the cracks are refined due to the incorporation of SSW. At the crack length/depth ratio of 0.25 and 0.5, the initial cracking load of RPC reinforced with 1.5% SSWs is increased by 170.0% and 183.1% respectively. Based on the TPFM calculation,

the increases of fracture toughness are determined as 151.7% and 203.4%, and the $CMOD_C$ is improved by 85.2% and 113.3%. According to DKFM calculation, the increases of initiation fracture toughness can reach 160.0% and 185.2%; meanwhile, the unstable fracture toughness is enhanced by 152.4% and 179.2%. The fracture energy of SSW reinforced RPC displays 440.5% and 1017.1% increments. The failure cracks of the composites become narrow, short and tortuous due to the increase of SSW content. The load-CMOD curves of SSW reinforced RPC under four-point shearing load include significant nonlinear ascending stage and obvious stationary stage before peak load. Compared with RPC without SSW, the mixed mode I-II fracture toughness of RPC reinforced with 1.5% SSWs is increased by 177.1% and 137.3% respectively at the crack length/depth ratio of 0.25 and 0.5. The four-point shearing initial cracking load of the composites is 222.3% and 112.0% higher than that of control RPC. The angle between mixed mode I-II crack and precast crack extension line is reduced, and the perpendicularity of shear cracks is improved with the increase of SSW volume fraction. The generation and propagation of cracks in the composites can be monitored by the variation of FCR under three-point bending and four-point shearing load.

The excellent fracture toughness of SSW reinforced RPC is of great significance for the improvement of structure safety in serviceability limit states. Meanwhile, the investigation on fracture parameters and mechanisms offers guidance for the construction design of SSW reinforced RPC. Moreover, the fracture self-sensing characteristics of the composites provide guidance for the development of large self-monitoring structures.

References

[1] Griffith A. A. The Phenomena of Rupture and Flow in Solids. Philosophical Transactions of the Royal Society of London, 1921,221(2):163-198.

[2] Kaplan M. F. Crack propagation and the fracture of concrete. American Concrete Institute, 1961,5(58):591-610.

[3] Jenq Y. S., Shah S. P. A Fracture toughness criterion for concrete. Engineering Fracture Mechanics, 1985,21(5):1055-1069.

[4] Swartz S. E., Taha N. M. Mixed mode crack propagation and fracture in concrete. Engineering Fracture Mechanics, 1990,35(1):137-144.

[5] Xu S., Reinhardt H. W. A simplified method for determining double-K fracture parameters for three-point bending tests.International Journal of Fracture, 2000,104(2):181-209.

[6] Zhao Y., Dong W., Xu B., et al. Effect of T-stress on the initial fracture toughness of concrete under I/II mixed-mode loading. Theoretical and Applied Fracture Mechanics. 2018,96: 699-706.

[7] Ghasemi M., Ghasemi M. R., Mousavi S. R. Investigating the effects of maximum aggregate size on self-compacting steel fiber reinforced concrete fracture parameters. Construction and Building Materials. 2018,162: 674-682.

[8] Kazemi M. T., Golsorkhtabar H., Beygi M. H. A., et al. Fracture properties of steel fiber reinforced high strength concrete using work of fracture and size effect methods. Construction and Building Materials. 2017,142: 482-489.

[9] Noaman A. T., Abu Bakar B. H., Akil H. M., et al. Fracture characteristics of plain and steel fibre reinforced rubberized concrete. Construction and Building Materials. 2017,152: 414-423.

[10] Sovják R., Máca P., Imlauf T. Effect of Fibre Length on the Fracture Energy of UHPFRC. Procedia Engineering. 2017,193: 74-79.

[11] Güneyisi E., Gesoglu M., Özturan T., et al. Fracture behavior and mechanical properties of concrete with artificial lightweight aggregate and steel fiber. Construction and Building Materials. 2015,84: 156-168.

[12] Mo K. H., Yap K. K. Q., Alengaram U. J., et al. The effect of steel fibres on the enhancement of flexural and compressive toughness and fracture characteristics of oil palm shell concrete. Construction and Building Materials. 2014,55: 20-28.

[13] Su C., Wu Q., Weng L., et al. Experimental investigation of mode I fracture features of steel fiber-reinforced reactive powder concrete using semi-circular bend test. Engineering Fracture Mechanics. 2019,209: 187-199.

[14] Xu M., Wille K. Fracture energy of UHP-FRC under direct tensile loading applied at low strain rates. Composites Part B: Engineering. 2015,80: 116-125.

[15] Köksal F., Şahin Y., Gencel O., et al. Fracture energy-based optimisation of steel fibre reinforced concretes. Engineering Fracture Mechanics. 2013,107: 29-37.

[16] Bencardino F., Rizzuti L., Spadea G., et al. Implications of test methodology on post-cracking and fracture behaviour of Steel Fibre Reinforced Concrete. Composites Part B: Engineering. 2013,46: 31-38.

[17] Dai X., Pu Q., Wang L., et al. Measurement on fracture process and prediction of the load capacity of steel fiber reinforced concrete by electronic speckle pattern interferometry. Composites Part B: Engineering. 2011,42(5): 1181-1188.

[18] Mudadu A., Tiberti G., Germano F., et al. The effect of fiber orientation on the post-cracking behavior of steel fiber reinforced concrete under bending and uniaxial tensile tests. Cement and Concrete Composites. 2018,93: 274-288.

[19] Pirmohammad S., Hojjati Mengharpey M. A new mixed mode I/II fracture test specimen: Numerical and experimental studies. Theoretical and Applied Fracture Mechanics. 2018,97: 204-214.

[20] Li G., Yu J., Cao P., et al. Experimental and numerical investigation on I–II mixed-mode fracture of concrete based on the Monte Carlo random aggregate distribution. Construction and Building Materials. 2018,191: 523-534.

[21] Xu Q., Dong W., Wu Z. M. Numerical Simulation on Mixed Mode I-II Crack Propagation Process in Concrete. Key Engineering Materials. 2008,385-387: 233-236.

[22] Le H. V., Moon D., Kim D. J. Effects of ageing and storage conditions on the interfacial bond strength of steel fibers in mortars. Construction and Building Materials. 2018, 170: 129-141.

[23] Hwang J. P., Kim M., Ann K. Y. Porosity generation arising from steel fibre in concrete. Construction and Building Materials. 2015,94:433-436.

[24] Bentur A., Mindess S. Fibre Reinforced Cementitious Composites[M]// Materials for Buildings and Structures, Volume 6. Wiley-VCH Verlag GmbH & Co. KGaA, 2006.

[25] Han B., Dong S., Ou J., et al. Microstructure related mechanical behavior of short-cut super-fine stainless wire reinforced reactive powder concrete. Materials and Design. 2016,96: 16-26.

[26] Dong S., Han B., Yu X., et al. Dynamic impact behavior and constitutive model of super-fine stainless wire reinforced reactive powder concrete. Construction and Building Materials. 2018,184: 602-616.

[27] Dong S., Han B., Yu X., et al. Constitutive model and reinforcing mechanisms of uniaxial compressive property for reactive powder concrete with super-fine stainless wire. Composites Part B: Engineering. 2019, 166: 298-309.

[28] Dong S., Han B., Ou J., et al. Electrically conductive behavior and mechanisms of short-cut super-fine stainless wire reinforced reactive powder concrete. Cement and Concrete Composites. 2016, 72: 48-65.

[29] Nguyen D. L., Song J., Manathamsombat C., et al. Comparative electromechanical damage-sensing behaviors of six strain-hardening steel fiber-reinforced cementitious composites under direct tension. Composites Part B: Engineering. 2015,69: 159-168.

[30] Kim D. J., Kim M. K., An Y. Electro-mechanical self-sensing response of ultra-high-performance fiber-reinforced concrete in tension. Composites Part B. 2018,134: 254-264.

[31] Sun S., Ding S., Han B., et al. .Multi-layer graphene-engineered cementitious composites with multifunctionality/intelligence. Composites Part B: Engineering. 2017, 129: 221-232.

[32] Han B., Ding S., Yu X. Intrinsic self-sensing concrete and structures: A review. Measurement[J]. 2015,59: 110-128.

[33] Han B., Yu X., Ou J. Self-Sensing Concrete in Smart Structures. Publisher: Elsevier. 2014.

[34] Richard P., Cheyrezy M. Composition of reactive powder concretes. Cement Concrete Research. 1995, 25(7):1501-1511.

[35] Carpinteri A., Fortese G., Ronchei C., et al. Mode I fracture toughness of fibre reinforced concrete. Theoretical and Applied Fracture Mechanics. 2017,91: 66-75.

[36] Stynoski P., Mondal P., Marsh C. Effects of silica additives on fracture properties of carbon nanotube and carbon fiber reinforced Portland cement mortar. Cement and Concrete Composites. 2015,55: 232-240.

[37] Kizilkanat A. B., Kabay N., Akyüncü V., et al. Mechanical properties and fracture behavior of basalt and glass fiber reinforced concrete: An experimental study. Construction and Building Materials. 2015,100: 218-224.

[38] Chen G. M., Yang H., Lin C. J., et al. Fracture behaviour of steel fibre reinforced recycled aggregate concrete after exposure to elevated temperatures. Construction and Building Materials. 2016,128: 272-286.

[39] Dong W., Zhou X., Wu Z. On fracture process zone and crack extension resistance of concrete based on initial fracture toughness. Construction and Building Materials. 2013,49: 352-363.

[40] Yu K., Yu J., Lu Z., et al. Determination of the softening curve and fracture toughness of high-strength concrete exposed to high temperature. Engineering Fracture Mechanics. 2015,149: 156-169.

[41] Hu Y., Luo D., Li P., et al. Fracture toughness enhancement of cement paste with multi-walled carbon nanotubes. Construction and Building Materials. 2014,70: 332-338.

[42] RILEM 50-FMC. Determination of the fracture energy of mortar and concrete by means of three-point bend tests on notched beams. Materials and Structures, 1985, (18): 287-290.

[43] Qian J. Three-point bending method for determination of fracture energy. China Concrete and Cement Products.1996(06):20-23.(In Chinese)

[44] Elices M., Guinea G.V., Planas J. Measurement of the fracture energy using three-point bend tests: part 3-influence of cutting the P–δ tail, Materials and Structures. 1992, (25): 137-163.

[45] Hu S., Hu L. Experimental Study of Shear Fracture of Concrete Specimens under 4-Point Loading. Journal of Yangtze River Scitific Institute. 2014, 31(9): 99-104. (In Chinese)

[46] Mirsayar M. M., Razmi A., Berto F. Tangential strain-based criteria for mixed-mode I/II fracture toughness of cement concrete. Fatigue and Fracture of Engineering Materials and Structures. 2018,41(1): 129-137.

[47] García-Macías E., D'Alessandro A., Castro-Triguero R., Pérez-Mira D., Ubertini F. Micromechanics modeling of the electrical conductivity of carbon nanotube cement-matrix composites. Compositr Part B: Engineering. 2017, 108: 451-469.

[48] Han B., Wang Y., Dong S., et al. Smart concrete and structures: a review. Journal of Intelligent Material Systems and Structures. 2015, 26(1):1303-1345.